Characterization of the ABC methionine transporter from *Neisseria meningitidis* reveals that MetQ is a lipoprotein

Naima G. Sharaf[1,2,*], Mona Shahgholi[1], Esther Kim[1], Jeffrey Y. Lai[1,2], David VanderVelde[1], Allen T. Lee[1,2], Douglas C. Rees[1,2,*]

***For correspondence:**
dcrees@caltech.edu (DCR);
ngsharaf@caltech.edu (NGS)

[1]California Institute of Technology, Division of Chemistry and Chemical Engineering 114-96, California Institute of Technology, Pasadena, CA 91125 USA; [2]Howard Hughes Medical Institute, California Institute of Technology, Pasadena, CA 91125, USA

Abstract NmMetQ is a substrate binding protein (SBP) from *Neisseria meningitidis* that has been identified as a surface-exposed candidate antigen for meningococcal vaccines. However, this location for NmMetQ challenges the prevailing view that SBPs in Gram-negative bacteria are localized to the periplasmic space to promote interaction with their cognate ABC transporter embedded in the bacterial inner membrane. To address the roles of NmMetQ, we characterized NmMetQ with and without its cognate ABC transporter (NmMetNI). Here, we show that NmMetQ is a lipoprotein (lipo-NmMetQ) that binds multiple methionine analogs and stimulates the ATPase activity of NmMetNI. Using single-particle electron cryo-microscopy, we determined the structures of NmMetNI in the absence and presence of lipo-NmMetQ. Based on our data, we propose that NmMetQ tethers to membranes via a lipid anchor and has dual function/topology, playing a role in NmMetNI-mediated transport at the inner-membrane in addition to moonlighting functions on the bacterial surface.

Introduction

The substrate binding protein NmMetQ from the human pathogen *Neisseria meningitidis* has been identified as a surface-exposed candidate antigen for the meningococcal vaccine (***Pizza et al., 2000***). Subsequently, NmMetQ was shown to interact with human brain microvascular endothelial cells (***Kánová et al., 2018***), potentially acting as an adhesin. However, the surface-topology of NmMetQ challenges the prevailing view that substrate binding proteins (SBPs) reside in the periplasm of Gram-negative bacteria (***Thomas and Tampé, 2020***), binding and delivering molecules to cognate ATP-Binding Cassette (ABC) transporters in the inner-membrane (IM). Several questions arise from these studies: Has NmMetQ lost its ABC transporter-dependent function in the IM? and How does NmMetQ become embedded in the outer membrane (OM) surface of the bacterium?

The ABC transporter-dependent role of SBPs has been well characterized for multiple ABC transporter systems (***Hollenstein et al., 2007***; ***Oldham et al., 2013***; ***Sabrialabed et al., 2020***; ***Liu et al., 2020***; ***Nguyen et al., 2018***; ***de Boer et al., 2019***). These studies reveal conserved SBP-dependent characteristics, including that the SBP is largely responsible for substrate delivery to the ABC transporter, with concomitant stimulation of the transport coupled ATPase activity. Structural studies have shown that SBPs dock to the periplasmic surface of the transporter's transmembrane

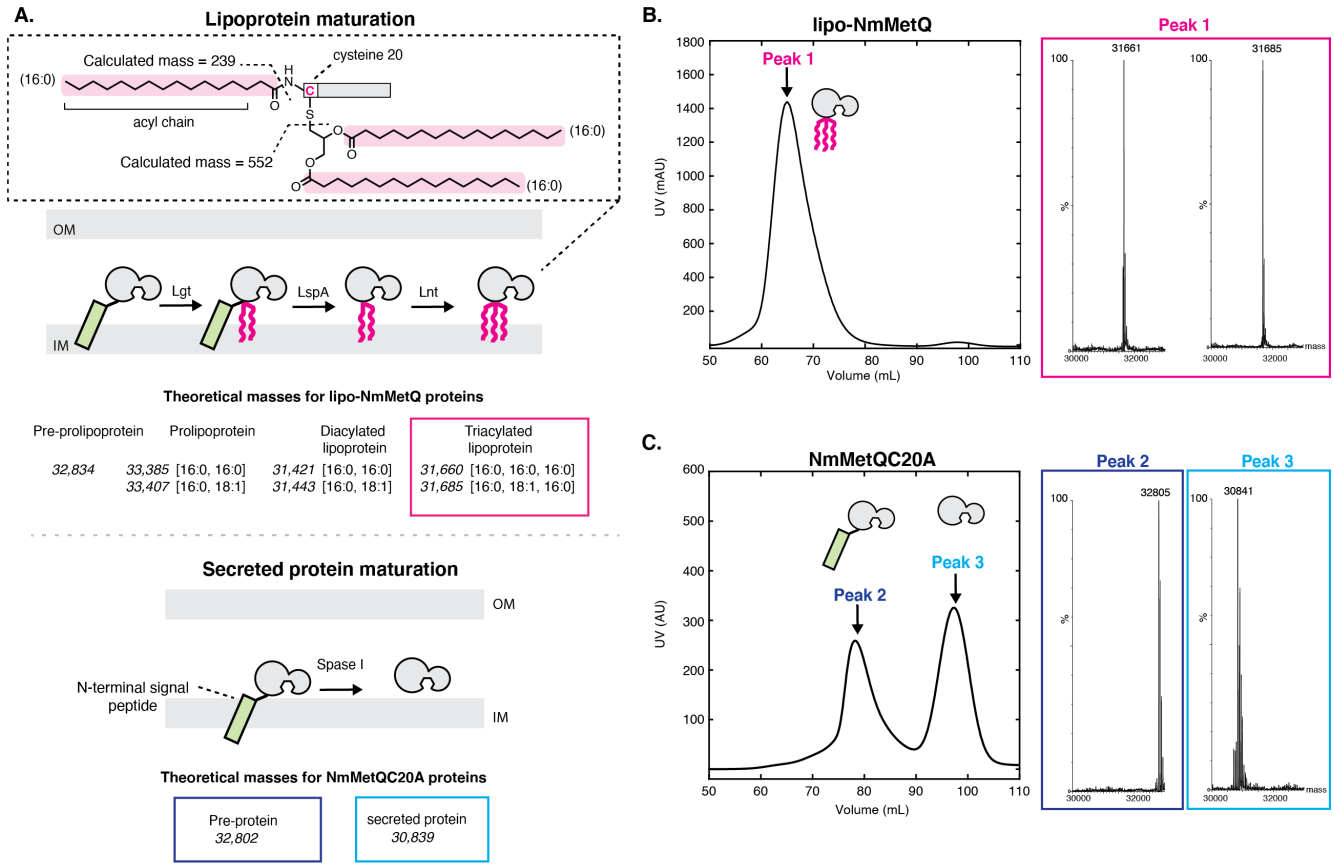

Figure 1. Mass spectrometry (MS) analysis of lipo-NmMetQ and NmMetQC20A proteins. A. (Top) Schematic pathway of lipoprotein maturation. Inset contains a schematic of a lipoprotein with acyl chain composition [16:0,16:0,16:0]. Acyl chains are grouped in a dotted line box and their average masses are calculated. Below the schematic are the theoretical masses for the lipo-NmMetQ proteins (in italics) assuming triacylation occurs via the canonical lipoprotein maturation pathway, due to the sequential action of three enzymes (Lgt, LspA and Lnt). The numbers in the brackets correspond to the total number of carbons and double bonds, respectively, present in the fatty acyl chains of the lipid. (Bottom) Schematic illustrating various NmMetQC20A proteins with example theoretical average masses, shown in italics, assuming cleavage occurs between A19 and A20, possibly by signal peptidase I (SPase I). N-terminal signal peptides are represented by a green rectangle. B. Characterization of lipo-NmMetQ. Size-exclusion chromatogram and mass spectra of peak 1. The molecular masses of the major species correspond within 1 Da to the predicted mass for two triacylated NmMetQ species, one with acyl chain composition [16:0, 16:0, 16:0] (31,661 Da) and the other with [16:0, 16:0, 18:1] (31,685 Da). C. Characterization of NmMetQC20A. Size-exclusion chromatogram and mass spectra of the major species from peak 2 and peak 3. The molecular masses of the major species of peak 2 and 3 correspond to the pre-protein NmMetQ (32,802 Da) and secreted NmMetQ (30,839 Da), respectively. These measured masses are within 3 Da of the predicted masses for each species. Assigned NmMetQ species are depicted in cartoon form on the chromatograms.

Figure 1–Figure supplement 1. DLS measurements of NmMetQ proteins

domains, with the substrate binding pocket juxtaposed with the translocation pathway of the transporter. While many SBPs have only been assigned ABC transporter-dependent functions, a few SBPs have also been shown to have both ABC transporter-dependent and ABC transporter-independent functions (often referred to as moonlighting functions) (**Adler, 1975**). For example, the *E. coli* maltose SBP (MBP) binds and stimulates its cognate ABC transporter (**Davidson et al., 1992**). In addition, the MBP-maltose complex is also a ligand for the chemotaxis receptor, triggering the signaling cascade involved in nutrient acquisition (**Hazelbauer, 1975**; **Manson et al., 1985**). Other SBPs have also been assigned ABC transporter-independent functions (**Müller et al., 2007**; **Castañeda-Roldán et al., 2006**; **Matthysse et al., 1996**), including NspS from *Vibrio cholerae* which has been shown to play a role in biofilm formation (**Young et al., 2021**) and not transport (**Cockerell et al., 2014**). Additionally, two MetQ proteins, *N. gonorrhoeae* (Ng) NgMetQ and *Vibrio vulnificus* (Vv) VvMetQ have also been identified as putative adhesins, mediating bacterial adhesion to human cervical epithelial cells (**Semchenko et al., 2016**) and to human intestinal epithelial cells (**Lee et al., 2010**; **Yu et al., 2011**), respectively. Evidence that these MetQ SBPs bind and stimulate their cognate ABC transporters, however, is lacking. Therefore, whether NmMetQ has lost its ATP transporter-dependent function, or plays dual roles at the IM and OM cannot be determined through amino acid sequence alone and must be experimentally verified.

Since SBPs are not membrane proteins, the detection of NmMetQ at the cell surface of the bacterium suggests it must be tethered to the OM. In Gram-negative bacteria, the paradigm that SBPs are translocated into the periplasm where they diffuse freely between the IM and OM can be traced back to early experiments by Heppel showing that the osmotic shock of Gram-negative bacteria leads to the release of SBPs (**Heppel, 1969**). While many SBPs in Gram-negative bacteria have been identified as secreted proteins (**Willis and Furlong, 1974**; **Ahlem et al., 1982**), several studies have also identified a few lipid-modified SBPs (lipo-SBP) (**Tokuda et al., 2007**)). However, the presence of lipo-SBPs in Gram-negative bacteria has not been generally appreciated (**Thomas and Tampé, 2020**) and the role that lipid modifications have on SBP surface-topology remains unexplored.

Although ABC transport-dependent functions of NmMetQ, VvMetQ and NgMetQ are not well studied, the homologous SBP from *E. coli* EcMetQ, is well characterized. Studies show that the *E. coli* methionine uptake system consists of EcMetQ and its cognate ABC transporter EcMetNI**Kadner** (**1974**, 1977). Structures of both EcMetQ and EcMetNI alone and in complex are available. (**Kadaba et al., 2008**; **Johnson et al., 2012**; **Nguyen et al., 2015**, **2018**). EcMetNI contains two transmembrane domains (TMD) that provide the substrate translocation pathway, together and two nucleotide binding domains (NBD) that couple transport to the binding and hydrolysis of ATP. In the absence of EcMetQ, EcMetNI adopts the inward-facing conformation, with the TMDs open to the cytoplasm and NBDs separated. The available crystal structures of EcMetQ reveal two domains connected by a linker that form the methionine binding pocket (**Nguyen et al., 2015**). Of note, EcMetQ has been experimentally verified to be a lipoprotein (**Tokuda et al., 2007**; **Carlson et al., 2018**). However, the lipid modification is not present in EcMetQ structures, since the the N-terminal signal sequence was removed from the constructs used to produce protein for crystallization (**Nguyen et al., 2015**). A structure of the EcMetQ-EcMetNI complex is also available and shows EcMetNI in the outward-facing conformation, with the TMDs and NBDs close together. In this structure, EcMetQ is docked to the periplasmic surface of the TMDs with the binding pocket open to the central cavity (**Nguyen et al., 2018**). These structures, together with *in vivo* functional assays (**Nguyen et al., 2018**; **Kadner, 1974**, **1977**), show that EcMetQ is intimately involved in EcMetNI-mediated methionine transport.

Whereas the interaction between EcMetQ and EcMetNI is well characterized, less is known about the corresponding system in *Neisseria meningitidis*. To date, there have been no biochemical or structural studies reported for NmMetNI. Recently determined structures of NmMetQ are in the ligand-free, L-methionine-, or D-methionine-bound states, and binding assays show L-methionine binds NmMetQ with greater affinity than D-methionine (**Nguyen et al., 2019**). These studies were carried out with an NmMetQ protein that lacks the native N-terminal signal sequence, establishing that the N-terminal signal sequence is not necessary for ligand binding. However, NmMetQ

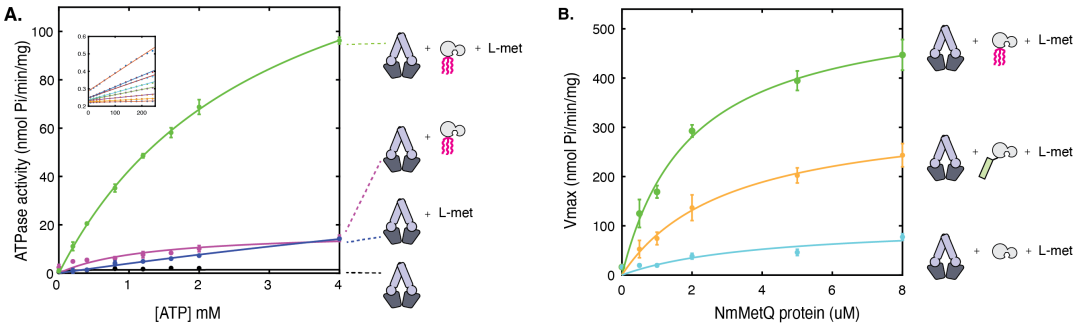

Figure 2. ATP hydrolysis of NmMetNI in the presence and absence of L-methionine and NmMetQ proteins. **A.** ATP hydrolysis was measured in the presence of 1 μM of DDM solubilized NmMetNI alone (black trace), 50 μM L-methionine (blue trace), 1 μM lipo-NmMetQ (magenta trace) and both 50 μM L-methionine and 1 μM lipo-NmMetQ (green trace). **B.** Specific activity of NmMetNI with increasing concentrations of various NmMetQ proteins: lipo-NmMetQ (green trace), pre-protein NmMetQ (orange trace) and secreted NmMetQ (cyan trace), and 50 μM L-methionine. N=3 error bars represent standard error of the mean (SEM). These data show the NmMetNI ATPase activity is tightly coupled, requiring both L-methionine and lipo-NmMetQ for maximal NmMetNI ATPase stimulation.

is predicted to be lipoprotein based on the N-terminal protein sequence (Uniprot entry Q7DD63) (***Consortium, 2019***). Experimental evidence confirming this modification, however, has not been reported. Thus, a full understanding of the post-translational modification of NmMetQ and its interactions with NmMetNI are lacking. To better understand NmMetQ and the role it plays in methionine transport, a detailed characterization of both NmMetNI and NmMetQ with its native N-terminal signal sequence is required.

In this work, we characterized NmMetNI and NmMetQ using multiple biophysical methods. Using mass spectrometry and site-directed mutagenesis, we demonstrate that full-length NmMetQ, recombinantly-expressed in *E. coli*, is a lipoprotein (lipo-NmMetQ). Functional assays show that both lipo-NmMetQ and L-methionine are required for maximal stimulation of NmMetNI ATPase activity. NmMetNI can also be stimulated, although to a lower extent, by L-methionine and pre-protein NmMetQ (a variant with an unprocessed N-terminal signal peptide), and lipo-NmMetQ and select methionine analogs. We also determined the structures of NmMetNI in the absence and presence of lipo-NmMetQ to 3.3 Å and 6.4 Å resolution, respectively, using single-particle electron cryo-microscopy (cryoEM). Using a bioinformatics approach, we also identified MetQ proteins from other Gram-negative bacteria that are predicted to be modified with lipids. This analysis suggests that the lipid modification of MetQ proteins are not restricted to *N. meningitidis* and *E. coli*.

Based on our data, we propose that lipo-NmMetQ, and more generally lipo-MetQ proteins in other Gram negative bacteria, have a dual function/dual topology: ABC transporter-dependent roles at the IM and a moonlighting ABC transporter-independent role (or roles) at the OM. Our findings highlight the complexity of the cell envelope and the need to more thoroughly characterize the rules that govern protein localization in Gram-negative bacteria and the moonlighting functions of SBPs that are present on the surface of the cell.

Results

N. meningitidis MetQ is a lipoprotein

While lipoproteins and secreted proteins both must traverse the inner cell membrane during biogenesis, their maturation occurs through different mechanisms depending the N-terminal signal sequence ***Figure 1***A. Lipoproteins are synthesized in the cytoplasm as pre-prolipoproteins, inserted in the IM, and then anchored via their N-terminal signal sequence to the cytoplasmic membrane (***Okuda and Tokuda, 2011***). While tethered to the IM through the signal sequence, pre-prolipoproteins are subsequently modified by three enzymes: (1) phosphatidylglycerol transferase (Lgt), that trans-

fers the diacylglycerol group preferentially from phosphatidylglycerol (PG) to the cysteine residue via a thioester bond of the pre-prolipoprotein, producing a prolipoprotein (***Mao et al., 2016***), (2) signal peptidase II (LspA), that cleaves the prolipoprotein N-terminal signal sequence to yield a di-acylated lipoprotein with the N-terminal cysteine (***Hussain et al., 1982***; ***Vogeley et al., 2016***), and (3) apolipoprotein N-acyl transferase (Lnt), that N-acetylates the cysteine residue to produce a tri-acylated lipoprotein preferentially using an acyl group of phosphatidylethanolamine (PE) (***Noland et al., 2017***; ***Wiktor et al., 2017***). Similar to lipoproteins, secreted proteins are synthesized in the cytoplasm as pre-proteins with an N-terminal signal sequence. These pre-proteins serve as substrates for signal peptidase I (Spase I), that cleaves the N-terminal signal sequence to yield the mature secreted protein (***Karla et al., 2005***; ***Paetzel et al., 1998***).

NmMetQ is predicted to be a lipoprotein by SignalP 5.0, a deep neural network algorithm that analyzes amino acid sequences to predict the presence and location of cleavage sites (***Armenteros et al., 2019***). To validate this prediction, we expressed NmMetQ using an *E. coli* expression system with the native N-terminal signal sequence and a C-terminal decahistidine tag. *E. coli* has been previously used to produce lipid modified *N. meningitidis* proteins (***Fantappiè et al., 2017***). We purified NmMetQ in the detergent n-dodecyl-β-D-maltopyranoside (DDM) using an immobilized nickel affinity column followed by size-exclusion chromatography (SEC). The SEC elution profile shows one main peak with an elution volume of 66 mL ***Figure 1***.A. An analysis of the peak fraction by liquid chromatography mass spectrometry (LC/MS) revealed two major deconvoluted masses of 31,662 and 31,682 Da ***Figure 1***.B. These masses correspond well with the theoretical masses of two lipoprotein NmMetQ proteins: one with a triacyl chain composition of 16:0,16:0 and 16:0 (31,661 Da) and another with a triacyl chain composition of 16:0,16:0 and 18:1 (31,685 Da), respectively ***Figure 1***.A (top). We calculated the intact masses of the lipo-NmMetQ proteins using a combination of 16:0 and 18:1 acyl chains because these were the major species found in previous studies of recombinantly expressed lipoproteins (***Hantke and Braun, 1973***; ***Luo et al., 2016***).

To confirm that lipid attachment site occurs at the N-terminal Cys 20 on NmMetQ, we generated a Cys-to-Ala NmMetQ mutant (NmMetQC20A). We hypothesized that this mutation would prevent lipid attachment and lead to the accumulation of pre-protein NmMetQ, containing an unprocessed N-terminal signal sequence and the C20A mutation. The NmMetQC20A protein was expressed and purified in DDM as previously described. The SEC elution profile reveals two major peaks with distinct elution volumes, 78 ml and 100 mL for peak 1 and 2, respectively ***Figure 1***C. For peak 1, analysis of the fraction containing the highest peak revealed a deconvoluted mass of 32,804, which correlates well with the theoretical intact mass of the pre-protein NmMetQ (32,802 Da). For peak 2 the deconvoluted mass was 30,840, which agrees with the theoretical intact mass of a secreted NmMetQ protein cleaved between Ala 19 and Ala 20 (30,839 Da) ***Figure 1***.A (bottom), respectively. The production of the secreted NmMetQ was surprising since we only expected the accumulation of the pre-protein NmMetQ. However, these data suggest that the Cys-to-Ala mutation created a noncanonical cleavage site, possibly allowing Spase I to inefficiently cleave the pre-protein to yield secreted NmMetQ. Together, these data clearly demonstrate that the major species of recombinantly-expressed NmMetQ is heterogeneously triacylated at Cys 20. Mutating Cys 20-to-Ala prevents the production of lipoprotein NmMetQ, leading to the formation of pre-protein NmMetQ and secreted NmMetQ. The location of cleavage site, position of lipid attachment, and hetergoenous triacyl chain composition of NmMetQ in this study are consistent with previous studies characterizing other lipoproteins produced in *E. coli* (***Luo et al., 2016***; ***Kwok et al., 2011***).

These data also reveal an interesting property of each DDM solubilized NmMetQ variant: lipo-NmMetQ, pre-protein lipo-NmMetQ, and secreted NmMetQ proteins elute at different volumes despite their similar molecular masses (between 31 and 33 kDa). Specifically, lipo-NmMetQ and pre-protein NmMetQ proteins elute at a much higher apparent mass than secreted NmMetQ on a Superdex 30/60 (GE healthcare) column ***Figure 1***.B,C. To further investigate the properties of the NmMetQ proteins, we used dynamic light scattering (DLS) to measure their hydrodynamic radii (R_h) and calculate their theoretical molecular weights assuming a folded globular protein. We found

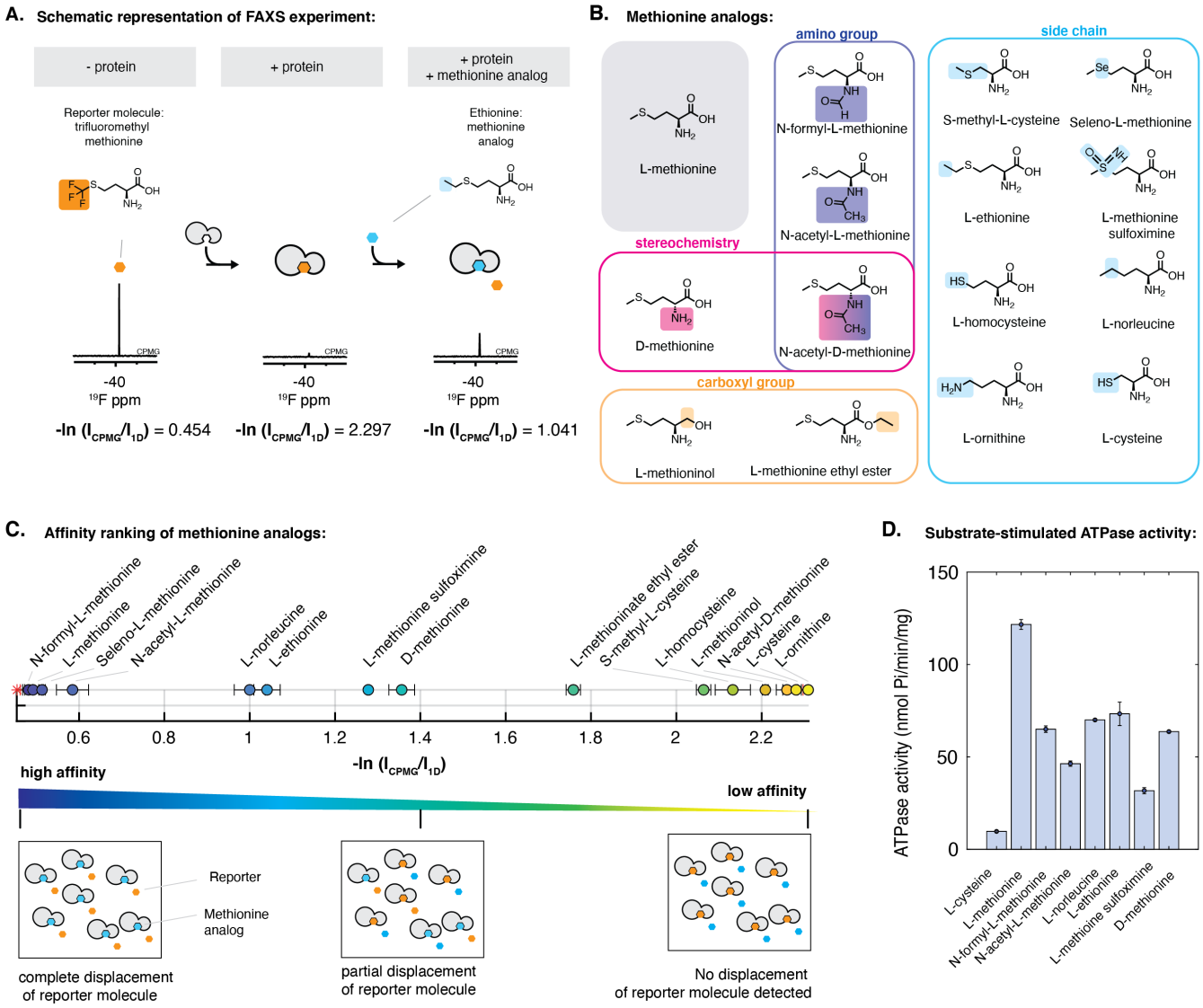

Figure 3. Characterization of the interaction of methionine analogs with NmMetQ using FAXS and ATPase experiments. **A.** Schematic diagram of the FAXS experiment. The intensity of the fluorine signal decreases in the presence of NLM-NmMetQ. Addition of the methionine analog causes the fluorine signal intensity of the reporter molecule to increase due to its displacement from NLM-NmMetQ. **B.** Chemical structures of the methionine analogs used in this study. **C.** (Top) Ordering of methionine analogs by their binding affinity to NLM-NmMetQ. (Bottom) Schematic representation of FAXS experiment depicted in bulk solution. Methionine analogs with higher affinity are positioned toward the left side of the plot, while lower affinity methionine analogs are positioned toward the right. **D.** ATPase activity NmMetNI at 2 mM ATP in the presence of lipo-NmMetQ and methionine analogs at 1:8:50 molar ratio, respectively. N=3 error bars represent SEM.

Figure 3–source data 1. The measured -ln(Icpmg/I1D) values: NMRtable.xlsx

that the R_h values and molecular weight estimates were larger for lipo-NmMetQ (R_h = 7.9 ± 0.17 nm, Mw-R = 430 ± 22 kDa) and pre-protein NmMetQ (R_h 7.7 ± 0.055 nm, Mw-R = 400 ± 6.7 kDa), than for secreted NmMetQ (R_h 3.0 ± 0.013 nm, Mw-R = 43 ± 0.33 kDa) (***Figure 1–Figure Supplement 1***). Based on both the size-exclusion chromatograms and DLS data, we propose that both lipo-NmMetQ and pre-protein NmMetQ aggregate to form micelles-like complexes.

The ATPase activity of NmMetNI is maximally stimulated in the presence of both lipo-NmMetQ and L-methionine

Figure 2.A shows that in the presence of 1 μM NmMetNI alone (black trace) and in the presence of 50 μM L-methionine (blue trace), the ATPase activity was low, demonstrating that L-methionine alone is not sufficient to stimulate NmMetNI ATPase activity. However, in the presence of both 1 μM lipo-NmMetQ and 50 μM L-methionine, a marked stimulation of ATPase activity was observed ***Figure 2***.A (green trace). To exclude the possibility that the stimulation of ATPase activity is mediated by either the lipid-moiety or the unliganded NmMetQ protein subunit, the experiment was repeated in the absence of L-methionine (NmMetNI and unliganded lipo-NmMetQ only), ***Figure 2***.A (magenta trace). Under these conditions the ATPase activity is low, showing that unliganded lipo-NmMetQ is not sufficient to stimulate NmMetNI activity. Given these findings, we conclude that NmMetNI ATPase activity is tightly coupled, requiring both L-methionine and lipo-NmMetQ for maximum stimulation. This data strongly suggests that lipo-NmMetQ plays a role in methionine-mediated NmMetNI ATP hydrolysis.

Next, we characterized the effect of different NmMetQ proteins (lipo-NmMetQ, pre-protein NmMetQ and secreted NmMetQ) on the ATPase activity of NmMetNI. ***Figure 2***.B, demonstrates that in the presence of 50 μM L-methionine, the NmMetNI ATPase activity increases with increasing concentration of lipo-NmMetQ up to 2 μM, after which the activity starts to plateau (green trace). The same protocol was performed with pre-protein NmMetQ, which contains an N-terminal signal sequence, but without the lipid modification. Addition of pre-protein NmMetQ also led to stimulation of ATPase activity, although to a lesser extent than observed for lipo-NmMetQ (orange trace). Addition of secreted NmMetQ, however, had little effect on the ATPase activity (cyan), however. Together, these data establish that the lipid moiety of lipo-NmMetQ is required for maximal NmMetNI stimulation, although the N-terminal signal sequence of pre-protein NmMetQ could partially mimic its stimulatory effect.

A comparison of NmMetNI's ATPase activity with that of the previously-characterized EcMetNI reveals that these transporters have different ligand-dependent ATPase activities. When L-methionine and SBP are absent, NmMetNI has no detectable basal ATP activity, however EcMetNI has a basal ATPase rate of 300 nmol Pi/min/mg (***Kadaba et al., 2008***). These transporters also differ in their response to L-methionine. In the presence of L-methionine, the ATPase activity of EcMetNI decreases due to the binding of L-methionine to the C2 domain, which is responsible for the regulatory phenomenon of transinhibition. For NmMetNI, however, no such effect was detected, as anticipated from the absence in NmMetNI of the C2 autoinhibitory domain.

A comparison of NmMetNI SBP-dependent ATPase stimulation to other ABC importers also reveals some similarities and differences. For NmMetNI, only liganded-SBP maximally stimulated NmMetNI ATP hydrolysis. Maximal stimulation by liganded-SBPs is also a mechanistic feature shared by the ABC importers EcMalFGK$_2$ (***Davidson et al., 1992***) and EcHisQMP$_2$ (***Ames et al., 1996***). In contrast, for the ABC importer EcYecSC-FliY, full stimulation of ATPase can be achieved in both the liganded-SBP and the unliganded-SBP (***Sabrialabed et al., 2020***). Although the origin of these differences are unclear, our data show that NmMetNI is tightly coupled and highlight the mechanistic differences between ABC importers.

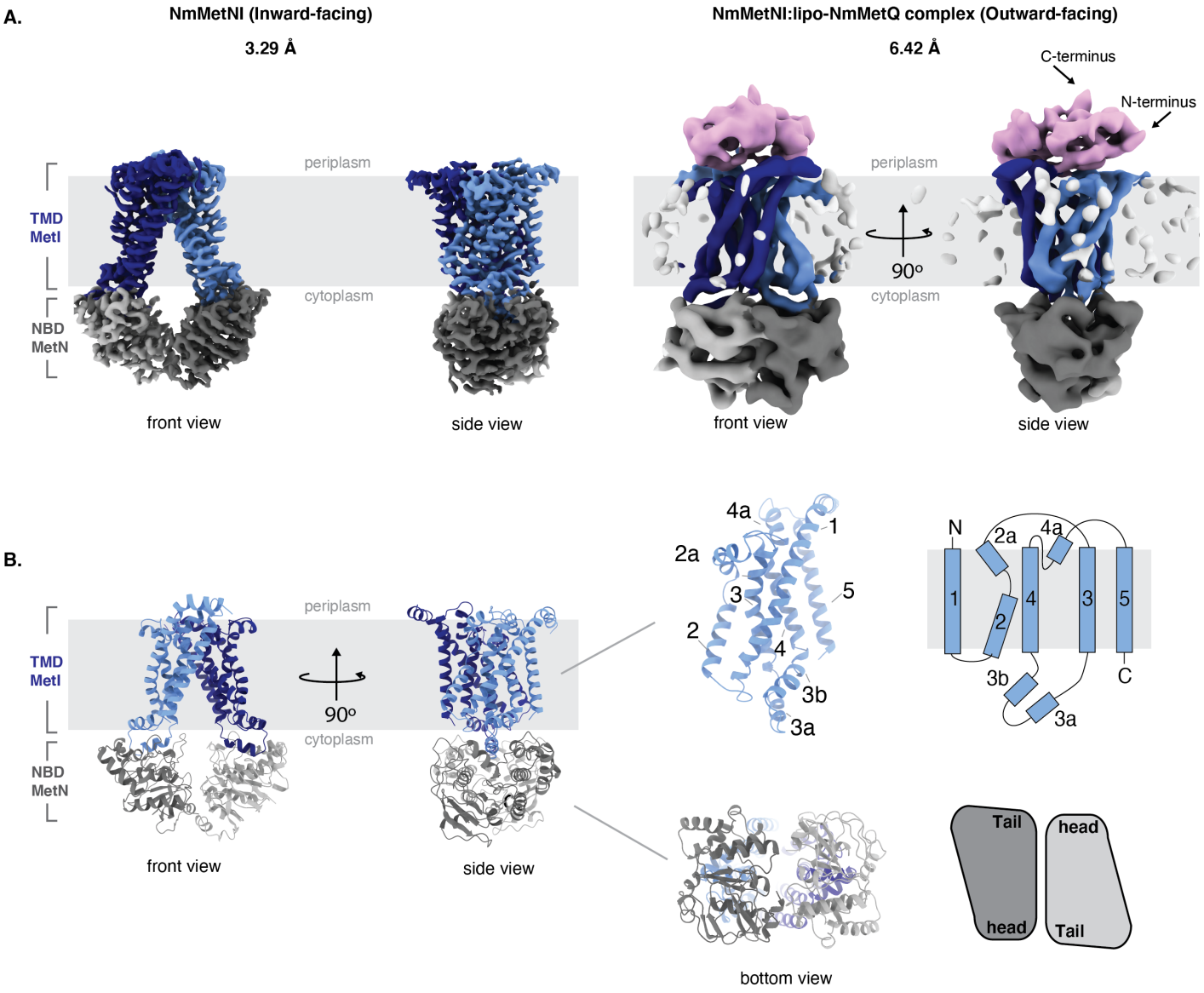

Figure 4. Architecture of NmMetNI and NmMetNI-lipo NmMetQ complex. A. The 3.3 Å resolution Cryo-EM map and NmMetNI in the inward-facing conformation in two views. B. Transmembrane topology of NmMetI, showing NmMetI contains five transmembrane helices per monomer C. The 6.4 Å resolution Cryo-EM map and model of NmMetNI in complex with lipo-NmMetQ in the presence of ATP. NmMetNI is in the outward-facing conformation. NmMetI is shown in light/dark blue, NmMetN in light/dark grey and lipo-NmMetQ in light pink. The membrane is represented by a grey box.

Figure 4–Figure supplement 1. CryoEM data collection and refinement statistics.

Figure 4–Figure supplement 2. Comparison of type I ABC transporters.

Figure 4–Figure supplement 3. CryoEM map generation and data processing refinement of NmMetNI in the inward-facing conformation.

Figure 4–Figure supplement 4. CryoEM map generation and data processing refinement of lipo-NmMetQ:NmMetNI complex in the outward-facing conformation.

N-formyl-L-methionine, L-norleucine, L-ethionine, and L-methionine sulfoximine are potential substrates for the lipo-NmMetQ:NmMetNI system

To identify potential substrates of the NmMetQ-lipoprotein MetQ system, we determined the relative binding affinities of several methionine analogs to NmMetQ. For these measurements, we used **F**luorine chemical shift **A**nisotropy and e**X**change for **S**creening (FAXS) in competition mode, a powerful solution NMR experiment that monitors the displacement of a fluorine-containing reporter molecule by a competing ligand. An important feature of FAXS is that fluorine modification of the competing ligand is not required (***Dalvit et al., 2003***; ***Dalvit and Vulpetti, 2018***). As previously discussed (***Gerig, 1994***; ***Dalvit and Vulpetti, 2018***), the fluorine nucleus has several properties that are advantageous for NMR: ^{19}F is 100% abundant, possesses a spin 1/2 nucleus, and has high gyromagnetic ratio, which results in high sensitivity (83 % of ^{1}H). It also has a large chemical shift anisotropy (CSA), allowing higher responsiveness to changes in molecular weight, such as those that occur during a protein-ligand binding event. Additionally, since fluorine atoms are not present in most commonly used buffer systems and virtually absent from all naturally occurring biomolecules, background interference in fluorine NMR experiments is minimal.

To optimize the FAXS experiment, we considered several factors. As shown in ***Figure 1***.B, lipoprotein NmMetQ may multimerize, possibly through an association with the hydrophobic acyl chains, increasing its apparent molecular weight. Because FAXS is sensitive to the apparent molecular weight of the protein, we chose to use a NmMetQ construct lacking its native N-terminal signal sequence and is therefore not modified with lipids (referred to here as NLM-NmMetQ). Trifluoromethylmethionine was selected as a reporter molecule and the fluorine signal intensity was monitored in the presence of NLM-NmMetQ and several methionine analogs (***Figure 3***.A). For these studies, we optimized the concentration of the reporter molecule, NLM-NmMetQ, and the relaxation time (T2) for the NMR measurement. A reporter molecule concentration of 2 mM was chosen here to decrease acquisition time. Additionally, 43 μM NLM-NMMetQ was chosen as a compromise between using less protein and increasing the fraction of reporter bound to the protein. The relaxation time T2= 120 ms was chosen for its ability to strongly attenuate but not eliminate the reporter signal in the presence of 43 μM NLM-NmMetQ. As previously described (***Dalvit et al., 2003***; ***Dalvit and Vulpetti, 2018***), for all experiments two fluorine spectra (1D and Car-Purcell-Meiboom-Gill (CPMG) filtered) were acquired. The intensity signals of the reporter molecule measured in both spectra and the ratio -ln(CPMG/1D) were calculated. We expected that analogs that bind to NLM-NmMetQ would lead to the displacement of the reporter molecule, resulting in a decrease in the -ln(CPMG/1D) ratio.

Our results for the competition binding experiments are shown in ***Figure 3***.C. The plot shows the signal intensity ratio of the reporter molecule in the presence of each methionine analog. Since displacement of the reporter molecule by the analog correlates to the analog's binding affinity, methionine analogs with higher affinity will be positioned toward the left side of the plot, while lower affinity methionine analogs will appear on the right side. As controls, we measured the -ln(CPMG/1D) ratios with the reporter molecule alone and reporter molecule plus NLM-NmMetQ. As expected, the reporter molecule alone has a low -ln(CPMG/1D) ratio, while the reporter molecule plus NLM-NmMetQ has a high -ln(CPMG/1D) ratio (less free reporter molecule due to NLM-binding). Next, we carried out the experiments in the presence of various methionine analogs. We first added L-methionine, a known high affinity ligand of NmMetQ (Kd 0.2 nM (***Nguyen et al., 2019***)). As expected for a higher affinity ligand, L-methionine completely displaced the reporter molecule. Next, we examined two methionine analogs with amino group substitutions: (1) N-acetyl L- methionine, which is present in bacteria (***Schmidt et al., 2016***) and human brain cells (***Smith et al., 2011***), and (2) N-formyl L-methionine, which is used by bacteria to initiate translation ***Figure 3***.C (circles). Addition of these analogs lead to the complete or near complete displacement of the reporter molecule, for N-formyl L-methionine and N-acetyl L-methionine respectively, indicating that changes to the amino group retain the ability to bind tightly to NLM-NmMetQ. D-methionine displaced less re-

porter than L-methionine, consistent with its lower binding affinity (3.5 μM (***Nguyen et al., 2019***)), while N-acetyl-D methionine failed to displace the reporter molecule. These results suggest that modifications to both the amino group and stereochemistry lead to significantly weaker binding than the singly modified derivative.

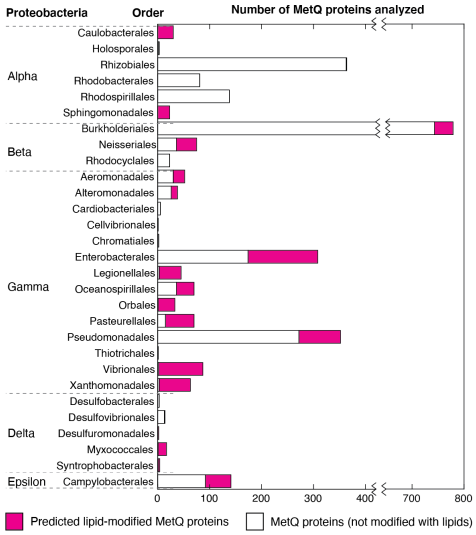

Figure 5. Distribution of lipid-modified MetQ proteins in different classes of Proteobacteria, a major phylum of Gram-negative bacteria. Plot of the number of MetQ proteins analyzed in each Order, grouped by Proteobacteria. Predicted lipid-modified and secreted MetQ proteins are shown in magenta and white, respectively.

Likewise, changes to the carboxyl group led to less displacement of the reporter molecule than L-methionine. Specifically, L-methioninol, with the carboxyl group reduced to an alcohol, failed to displace the reporter molecule while L-methionine ethyl ester only partially displaced the reporter molecule. Finally, changes to the L-methionine side chain exhibited varying effects. Methionine analogs with changes to the sulfur atom, including seleno-L-methionine, L-methionine sulfoximine, and L-norleucine were well tolerated, with a greater displacement of the reporter molecule than D-methionine, which has an estimated Kd of 3.5 μM (***Nguyen et al., 2019***). However, L-ornithine failed to displace the reporter molecule, suggesting that binding of ligands with a charged amino group is energetically unfavorable. Side-chain length also plays a role in methionine analog affinity to NLM-NmMetQ. Increasing the side-chain length by an addition of a methyl group (L-ethionine) was better tolerated than decreasing the length by one carbon (S-methyl-L-cysteine). Shorter thiol derivatives (L-cysteine and L-homocysteine) were ineffective at displacing the reporter molecule. Together, these data establish that NLM-NmMetQ can accommodate variability in the binding of methionine analogs, including modifications to the amino group, D-stereochemistry, and to a more limited extent, changes in the side-chain, while exhibiting little tolerance for variations in the carboxyl group.

To determine whether methionine analogs could serve as potential substrates for the lipo-NmMetQ NmMetNI system, we then measured NmMetNI ATPase activity in presence of lipo-NmMetQ and several methionine analogs. For these assays, we chose several methionine analogs identified by FAXS to bind NLM-NmMetQ with an affinity similar or higher than D-methionine, a known substrate for *E. coli* NmMetNI. Since substrate stimulated ATPase activity is a hallmark of ABC transporters (***Bishop et al., 1989***; ***Mimmack et al., 1989***), we expected methionine analogs that are substrates for this system would stimulate NmMetNI ATPase activity. ***Figure 2*** shows the results for the methionine analog stimulation of NmMetNI ATPase activity. As a negative control, we tested L-cysteine, where, as expected, no substrate-stimulated ATPase stimulation was detected. Our data shows that the following methionine analogs led to substrate-stimulated ATPase activity: N-acetyl L-methionine, N-formyl-L-methionine, L-norleucine, L-ethionine, and L-methionine sulfoximine. However, no correlation was seen between affinity to NLM-NmMetQ and NmMetNI stimulation. This data suggest that binding to NmMetQ is necessary to initiate transport; however, this step alone does not determine the magnitude of NmMetNI ATPase stimulation. Together, the FAXS and ATPase experiments suggest that N-formyl-L-methionine, L-norleucine, L-ethionine, and L-methionine sulfoximine are potential substrates for the *N. meningitidis* lipo-NmMetQ:NmMetNI system.

Structures of *N. meningitidis* MetNI in the inward-facing conformation and *N. meningitidis* MetNI:lipo NmMetQ complex in the outward-facing conformation

To gain insight into the potential role of lipo-NmMetQ in the NmMetNI transport cycle, we determined structures of NmMetNI in different conformational states by single-particle cryoEM. Multiple conditions were screened to identify ones that promoted lipo-NmMetNI-NmMetQ complex formation. Unexpectedly, these conditions did not always reveal structures of NmMetNI complex in complex with lipo-NmMetQ. In the presence of lipo-NmMetQ and AMPPNP, only a structure of NmMetNI in the inward-facing conformation at 3.3 Å resolution ***Figure 4–Figure Supplement 1*** was captured: no densities for either AMPPNP and lipo-NmMetQ, ***Figure 4*** were seen. For this data set, the two dimensional class averages showed clear structural features, suggesting a high level of conformational homogeneity ***Figure 4–Figure Supplement 3***. The overall architecture of NmMetNI is similar to previously determined structures of EcMetNI, comprising two copies of each TMD and NBD, encoded by *MetI* and *MetN*, respectively (***Kadaba et al., 2008***; ***Johnson et al., 2012***). Each MetI subunit contains five transmembrane helices per monomer for a total of ten transmembrane helices per transporter ***Figure 4***.

A comparison between NmMetNI and EcMetNI reveals similar subunit folds, with the root mean square deviation (RMSD) of 2.4 Å over 843 Cα atoms. As predicted from the primary sequence, the NmMetN subunits lack the C2 autoinhibitory domain. As a result, the interfaces of NmMetNI and EcMetNI are distinct. In the inward-facing conformation of NmMetNI, the NBDs interact directly. In contrast, in EcMetNI, the inward-facing conformation forms an interface through the C2 autoinhibitory domains, with a slight separation between the NBDs ***Figure 4–Figure Supplement 1***.A. A similar increase in NBD:NBD distance, defined as the average distance between Cα of glycines in the P loop and signature motifs, is observed the previously determined molybdate ABC transporter structures, *Methanosarcina acetivorans* ModBC (MaModBC) and *Archaeoglobus fulgidus* ModBC (AfModBC) (***Hollenstein et al., 2007***; ***Gerber et al., 2008***) ***Figure 4–Figure Supplement 1***.B. To date, these are the only other reported pair of homologous structures, one with an autoinhibitory domain and one without. For AfModBC, which lacks the autoinhibitory domain, the NBD:NBD distance is $\sim$ 17 Å and 21 Å for each AfModBC in the asymmetric unit. For MaModBC, which does have an autoinhibitory domain, this distance increases to $\sim$ 27 Å. A comparison of these four structures suggest that type I ABC importers share a common quaternary arrangement in the inward-facing conformation such that the presence of a regulatory domain increases the separation of the NBD:NBD distance in comparison to the homologous structure without a regulatory domain.

We also determined the single-particle cryoEM structure of DDM solubilized NmMetNI in complex with lipo-NmMetQ in the presence of ATP to 6.4 Å resolution ***Figure 4–Figure Supplement 1***.A. This structure was modeled by rigid-body refinement of both NmMetNI in the inward-facing conformation (traced from the 3.3 Å resolution reconstruction) and the previously determined soluble NmMetQ structure in the substrate free conformation (PDB:6CVA). Our model shows lipo-NmMetQ docked onto the NmMetI subunits and the NmMetN subunits in a closed dimer state. No clear density was seen for the lipid anchor of lipo-NmMetQ or ATP ***Figure 4***. A comparison between NmMetNI and EcMetNI in the outward-facing conformation in complex with their respective MetQ proteins reveals they have similar conformations, with RMSD of 2.2 Å over 1048 Cα atoms ***Figure 4–Figure Supplement 1***.C. In contrast to the inward-facing conformation, the NBD:NBD arrangement is similar for both EcNmMetQ and NmMetNI.

Lipo-MetQ proteins may be present in a variety of other Gram-negative bacteria

We used a bioinformatics approach to determine if other Gram-negative bacteria could have lipid-modified MetQ proteins. For the analysis, we chose predicted MetQ protein sequences from the InterPro family IPR004872 (of which NmMetQ is a member), restricting the search to Proteobacteria, Taxonomy ID 1224 and 90% identity. The amino acid sequence of the MetQ proteins were then analyzed using SignalP 5.0. ***Figure 5*** summarizes the results. Our data reveals that lipid-modified MetQ proteins may be present in all classes of Proteobacteria (Alpha, Beta, Gamma, Delta and Ep-

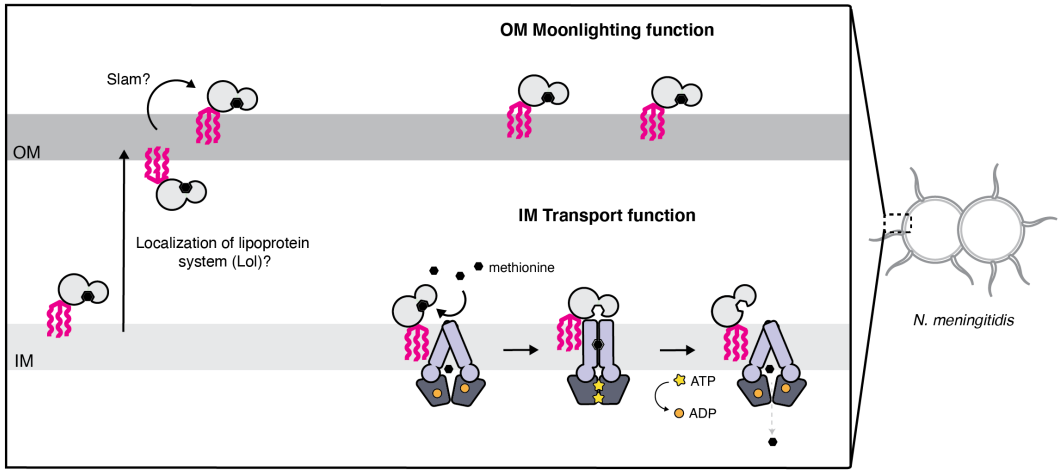

Figure 6. Proposed model for the cellular distribution of the *N. meningitidis* ABC methionine transporter proteins. Lipo-NmMetQ tethers to membranes via a lipid anchor and has dual function/topology, playing a role in NmMetNI-mediated transport at the inner-membrane in addition to moonlighting functions on the bacterial surface. The lipid modifications are central to the model, helping to explain how NmMetQ remains at the surface of the bacterium.

silon), with a varying number of lipid-modified MetQ proteins in each Order (magenta vs white). These results suggest that lipid modification of MetQ proteins are not restricted to *N. meningitidis*(this work) and *E. coli*(***Tokuda et al., 2007***; ***Carlson et al., 2018***) and are likely present in a wide variety of Gram-negative bacteria.

Discussion

NmMetQ has been previously identified as an OM surface-exposed candidate meningococcal vaccine antigen (***Pizza et al., 2000***), possibly playing a role in bacterial adhesion to human brain endothelial cells (***Kánová et al., 2018***). However, the presence of NmMetQ at the OM challenges the prevailing view that SBPs reside in the periplasm, freely diffusing between the IM and OM (***Thomas and Tampé, 2020***). To better understand whether NmMetQ has lost its ABC transporter-dependent function at the IM and how NmMetQ remains at the surface of the bacterium, we used multiple biophysical techniques to characterize the structure and function of NmMetQ and NmMetNI. Here, we show that NmMetQ is a lipoprotein that binds and stimulates NmMetNI.

Based on our data, we propose a model for NmMetQ localization that reconciles previous studies identifying NmMetQ as a surface-exposed candidate antigen and our study characterizing NmMetQ as a cognate SBP to NmMetNI. In our model, NmMetQ is a lipoprotein with dual function/topology ***Figure 6***. In this model, lipo-NmMetQ plays a role in nutrient acquisition at the IM. Lipo-NmMetQ is then transported to the OM, possibly through the localization of the lipoprotein system (Lol) (***Zückert, 2014***), and then flipped to the surface of the cell via Slam (a protein involved in lipoprotein surface exposure in *N. meningitidis*) (***Hooda et al., 2016***). Lipo-NmMetQ then anchors to the OM cell-surface via its lipid moiety, playing a role in adhesion. The lipid modifications are central to our model, helping to explain how NmMetQ remains at the surface of the bacterium.

Our identification of NmMetQ as a lipoprotein is predicated on our ability to express and purify lipo-NmMetQ and its processing variants. We recognize that a key assumption in our study is that the *E. coli* and *N. meningitidis* lipoprotein maturation machineries process the N-terminal signal sequences of lipoproteins in a similar manner. Since previous studies have successfully expressed in *E. coli* lipoproteins with their native signal sequences from other Gram-negative bacteria (***Parra et al., 2010***; ***Hooda et al., 2016***), including two lipoproteins from *N. meningitidis* (***Fantappiè et al., 2017***), we reasoned that these biochemical pathways are sufficiently similar between *E. coli* and *N. meningitidis* to justify this assumption .

Our ability to express and purify lipo-NmMetQ, pre-protein NmMetQ and secreted NmMetQ allowed us to carry out *in vitro* studies investigating whether NmMetQ can function as a SBP for NmMetNI. Functional assays show that both lipo-NmMetQ and L-methionine are required for maximal ATPase stimulation of NmMetNI. NmMetNI can also be stimulated, although to a lower extent, by pre-protein NmMetQ/L-methionine, and lipo-NmMetQ/select methionine analogs. Binding of lipo-NmMetQ to NmMetNI was also investigated by determining the cryoEM structures of NmMetNI in the presence and absence of lipo-NmMetQ. Our structures show lipo-NmMetQ binds to the TMDs of NmMetNI, similar to that of well-characterized *E. coli* ABC methionine transporter system, EcMetNI-EcMetQ (***Nguyen et al., 2018***). Together, our data suggests that lipo-NmMetQ plays a role in NmMetNI-mediated nutrient acquisition.

The dual functionality of SBPs may help explain why the intracellular concentrations of SBPs are typically ∽20x that of their cognate ABC transporters, depending on growth conditions (***Schmidt et al., 2016***). Of particular note, under many of the tested growth conditions, MetQ was the most abundant SBP in *E. coli*, present at up to nearly 30,000 copies per cell; for comparison MetNI was typically present at 1,000 copies per cell. A tempting interpretation of this observation is that larger number of SBPs increases the efficiency of nutrient uptake. Given that methionine is a scarce amino acid in human nasopharynx (where *N. meningitidis* primarily colonize (***Stephens et al., 2007***)) (***Krismer et al., 2014***) and one most expensive amino acid to synthesize in terms of ATP requirement (as measure in *E. coli*) (***Kaleta et al., 2013***), having multiple copies of NmMetQ may enable *N. meningitidis* to more efficiently capture methionine from the nutrient limited environment.

However, our study raises the possibility that higher SBPs concentrations may also reflect their participation in ABC transporter-independent functions, including moonlighting functions at the surface of the cell. As a consequence, the stoichiometry of SBPs to cognate ABC transporters measured in (***Schmidt et al., 2016***) may be misleading if the SBPs are distributed between multiple locations, in addition to the periplasmic space. Our study also calls for caution in interpreting SBP gene knock-out experiments, since the deletion of SBPs genes may led to phenotype(s) associated with the loss of either or both ABC transporter-dependent and -independent SBP functions.

While previous studies have shown that many SBPs of Gram-negative are soluble (***Heppel, 1969***), our findings suggest that at least some SBPs may be modified with lipids. Since lipid modifications may allow for SBPs to have a surface-topology in Gram-negative bacteria, we believe that future efforts should be made to experimentally determine which SBPs have lipid modifications, dual topology, and ABC transporter-independent functions. Studies aimed at determining the rules that govern protein surface-exposure will not only increase our understanding of bacterial physiology, but will also help in the rational design of vaccines based on surface-exposed protein antigens.

Methods and Materials

Cloning, expression and purification of *N. meningitidis* proteins

The protein encoding genes of MetQ and MetNI were obtained from *N. meningitidis* virulent strain MC58, GeneBank accession number AE002098. To produce MetNI, the DNA sequences encoding both MetN and MetI were inserted into a single modified pET vector, each under the control of a separate T7 promoter. To aid expression and purification, a decahistidine plus enterokinase site MGHHHHHHHHHHSSGHIDDDKH sequence was added to the N-terminus of MetN, while MetI contained no additional residues. A similar strategy was used to produce other ABC transporters.(***Locher et al., 2002***; ***Pinkett et al., 2007***). To produce lipo-NmMetQ, the DNA sequence encoding the NmMetQ with the native signal sequence and a C-terminal decahistidine tag was added to a single modified pET vector. This construct served as a template to generate the C20A mutant, which was created using PCR site-directed mutagenesis. NLM-NmMetQ was created as previously described (***Nguyen et al., 2019***).

All proteins were expressed in *E. coli* BL21 (DE3) gold (Agilent Technologies, Santa Clara, CA) cells using autoinduction media (***Studier, 2005***) by growing cells for 48 h at 22 °C. Cells were har-

vested by centrifugation and stored at -80 °C. To purify lipo-NmMetQ, NmMetQC20A proteins (pre-protein and secreted NmMetQ) and the transporter NmMetNI, 10 grams of frozen cell paste were thawed and homogenized in 100 mL of ice cold lysis buffer 25 mM Tris, pH 7.5, 100 mM NaCl, 40 mg of lysozyme, 4 mg DNase and one Complete Protease Inhibitor Cocktail Tablet (Roche Diagnostics GmbH). Cells were lysed by the addition of 1% v/w n-dodecyl-β-D-maltopyranoside (DDM, Anatrace) and by stirring the homogenate for 3 hr at 4 °C. Cell debris was removed by 45,000 rpm centrifugation for 45 min. Proteins were purified using a 5 mL HisTrap HP column (GE healthcare) followed by gel filtration (Superdex 30/60 GE healthcare).

Dynamic light scattering

DLS measurements were performed using a DynaPro NanoStar instrument (Wyatt Technology) using the manufacturer's suggested settings. A disposable UVette cuvette (Eppendorf) was used to contain the samples. Each sample was analyzed in triplicate to yield an average and standard deviation. Dynamics 7.1.7 software was used to analyze the data.

Single-particle CryoEM

UltrAufoil 1.2/1.3, 300 mesh grids (Electron Microscopy Sciences) were glow-discharged for 60 s at 15 mA using a PELCO easiGLOW (Ted Pella). Samples were then incubated at 37 ÅC for 5 min and then applied to the grids (3 μL), blotted with Whatman No.1 filter paper for 4 s with a blot force of 0 at 22 ÅC and 100 % humidity and plunge-frozen into liquid ethane using a Mark IV Vitrobot (Thermo Fisher). The grids were then stored in liquid nitrogen until further use.

Data collection was performed in a 300-KeV Titan Krios transmission electron microscope (Thermo Fisher Scientific) at the cryoEM facility at Caltech in Pasadena, California. Movies were collected using SerialEM v.3.7 automated data collection software (***Mastronarde, 2005***) with a beam-image shift over a 3-by-3 pattern of 1.2 μm holes with 3 exposures per hole in super-resolution mode (pixel size of 0.428 Å px^{-}) on a K3 camera (Gatan).

Image processing

Data collection parameters are summarized in ***Figure 4–Figure Supplement 1***. The data-processing workflow described below was performed for all datasets using cryoSPARC v.2.15 (***Punjani et al., 2017***). CryoEM movies were patch motion corrected for beam-induced motion including dose weighting with cryoSPARC after binning super-resolution movies. The non-dose-weighted images were used to estimate CTF parameters using Patch CTF job in cryoSPARC. Micrographs containing either ice or poor CTF fit resolution estimations were discarded. A subset of images was randomly selected and used for reference-free particle picking using Blob picker. Particles were subjected to multiple rounds of 2D classification, and two classes (top and side) were used as templates for particle picking on the full set of images. The subsequent processing steps were different for the two datasets.

For the dataset acquired for NmMetNI in the inward-facing conformation, initial particle stacks were extracted, downsampled four times, and then subjected to 2D classification. Classes that were interpreted as junk were discarded. The selected particles were then used to generate *ab initio* volumes. Two volumes, interpreted as NmMetNI and a junk/noise class, were selected for heterogeneous refinement. Particles assigned to the NmMetNI class were processed further by repeating the same strategy using particles downsampled twice, and then again with no downsampled particles. The final resulting particle stack was then non-uniformly refined (***Figure 4–Figure Supplement 3***).

For the dataset acquired for the lipo-NmMetQ:NmMetNI complex in the outward-facing conformation, initial particle stacks were extracted, downsampled ten times and subjected to 2D classification. Classes that were interpreted as junk were discarded. 2D classification was then repeated with particles downsampled by four, and then again with no downsampled particles. The

selected particles were then used to generate *ab initio* volumes. Two volumes, interpreted as lipo-NmMetQ:NmMetNI complex and junk/noise classes were selected for heterogeneous refinement. Particles assigned to the lipo-NmMetQ:NmMetNI complex class were subjected to another round of *ab initio*, followed by heterogeneous, refinement. The final resulting particle stack was then non-uniformly refined (***Figure 4–Figure Supplement 4***).

To build the atomic model of NmMetNI in the inward-facing structure, the structure of EcMetNI (PDB: 3TUJ) lacking the C2 domain was used as template for model building. The model was built by rigid-body docking, homology modeling, and manually building into the 3.3 Å resolution cryoEM density in Coot v0.9.1 (***Emsley et al., 2010***) and refined using ISOLDE (***Croll, 2018***). The model of the NmMetNI:lipo-NmMetQ complex in the outward-facing conformation was built by rigid-body refinement of NmMetNI in the inward-facing conformation (traced from the 3.3 Å resolution reconstruction) and of the previously determined soluble NmMetQ structure in the substrate free conformation (PDB:6CVA) were used as template for model building. The model was built by rigid-body docking in Coot, followed by refinement in ISOLDE using adaptive distance restraints.

Intersubunit distances between ATP-binding domains were defined by the positions of Cα of glycine residues of the P loop and signature motifs like previously described (***Kadaba et al., 2008***). Specifically, Gly44/Gly144 and Gly43/Gly143 for NmMetNI and EcMetNI (3TUJ), respectively and Gly36/Gly129 and Gly38/Gly130 for AfModBC(2ONK) and MaModBC(3D31), respectively. For each transporter, two intersubunit distances were measured and averaged using UCSF Chimera version 1.1 (***Pettersen et al., 2021***; ***Goddard et al., 2018***).

RMSD measurements were carried out using Coot v0.9.1 using SSM Superposition using default settings (***Krissinel and Henrick, 2004***). All images of models and densities were prepared using UCSF Chimera version 1.1.

MS analysis

The molecular masses of the proteins were determined by Ultra-Performance Liquid Chromatography-Mass Spectrometry (UPLC-MS) method. The UPLC-MS consisted of a Waters Acquity™ Chromatography platform and a Waters LCT Premier XE mass spectrometer. The chromatography separations used a solvent system of 0.1 % formic in water (solvent A) and 0.1 % formic acid in acetonitrile (solvent B), with a 10 m solvent program that reached 95 % B at 7 m. UPLC solvent flow was 0.4 mL/m from 0-1 m for desalting and was subsequently reduced to 0.22 mL/m. Samples dissolved in 25 mM Tris HCl pH 7.5, 100 mM NaCl, 0.05 % DDM were injected onto a Waters BEH C4 1.7 μ 300 Å 50 mm long ∽2.0 mm internal diameter column connected directly to the mass spectrometer. Electrospray ionization (ESI) was used in positive ion mode. The mass spectrometer was operated in the V Mode.

ATPase experiments.

Activity assays were performed in an Infinite 200 microplate reader (Tecan) at 37 °C using the EnzChek phosphate assay kit (ThermoFischer Scientific) to measure the amount of inorganic phosphate. Each 100 μL reaction contained 5 μM NmMetNI, 20 mM Tris-HCl pH 7.5, 100 mM NaCl, 5 mM β-mercaptoethanol, 200 μM 2-amino-6-mercapto-7-methylpurine riboside substrate, 0.1 units of purine nucleoside phosphorylase, and 0.05% DDM. NmMetQ proteins, and L-methionine was present as indicated in the figure captions. Samples were incubated for 15 minutes at 37 °C and the reactions were then initiated by an automatic injection of $MgCl_2$ to a final concentration of 5 mM. Initial rates were determined using Matlab software by calculating the linear portion of the change in absorbance at 360 nm as a function of time following the injection of $MgCl_2$.

NMR

^{19}F-NMR spectroscopy All NMR spectra were recorded at 300 K with a Bruker Ascend 400 NMR spectrometer equipped with multinuclear iProbe (^{1}H/^{19}F, ^{31}P-^{109}Ag) and a 24 position sample changer. CPMG relaxation dispersion ^{19}F spectra were recorded with a T_2 of 1 ms before the acquisition

period and 120 ms between the train of 180 °C- pulses. Free induction decay (FID) signals were backward linear predicted to 11 points and apodized with a 1.5 Hz Lorentzian filter. The spectra were analyzed with MestReNova v12.0.2 (Mestrelab Research), and intensity values were performed using the Line Fitting tool. Trifluoromethyl methionine was synthesized and purchased from Peptech (Bedford, MA). For the competition experiments, each sample contained 43 μM *N. meningitidis* MetQ, 2 mM trifluoromethyl methionine (reporter molecule), and 43 μM methionine analog (competing molecule).

Bioinformatics

Protein sequences were obtained through the UniProtKB database using the following search terms: Proteobacteria (taxonomy ID 1224), InterPro family IPR004872 (which NmMetQ UniProt ID Q7DD63 is a member) and identity 90%, which groups sequences with > 90 % identity and 80 % sequence length. SignalP 5.0 was used separately to analyze the N-terminal protein sequences and predict the location of the signal sequence cleavage sites. Sequence alignment data was generated by the EFI Enzyme Similarity Tool (https://efi.igb.illinois.edu/efi-est/) using Option C with FASTA header reading (***Gerlt et al., 2015***). A SSN network was then created using an alignment score corresponding to approximately 60% sequence identity and filtering for sequences between 240 and 330 residues in length. Cytoscape v3.8.0 (***Smoot et al., 2011***) was used for visualizing lipo-MetQ trends and obtaining taxonomy information. The table was exported and graphed in Matlab (MathWorks).

Data availability

For NmMetNI in the inward-facing conformation and lipo-NmMetQ:NmMetNI complex in the outward-facing conformation, cryoEM maps have been deposited in the Electron Microscopy Data Bank (EMDB) under accession codes EMD-23752 and EMD-23751. Coordinates for the model are deposited in the Research Collaboratory for Structural Bioinformatics Protein Data Bank under accession numbers 7MC0 and 7MBZ, respectively.

Acknowledgments

We thank Jacob Parres-Gold and Dr. Sara J. Weaver for useful discussions and Dr. Lilien Voong for critical reading of the manuscript. We also thank the staff at the Beckman Institute Resource Center for Transmission Electron Microscopy at Caltech for assistance with data collection. N.G.S was supported by the Postdoctoral Enrichment Program from the Burroughs Wellcome Fund and D.C.R is a Howard Hughes Medical Institute Investigator.

References

Adler J. Chemotaxis in bacteria. Annual Review of Biochemistry. 1975; 44(1):341–356.

Ahlem C, Huisman W, Neslund G, Dahms A. Purification and properties of a periplasmic D-xylose-binding protein from *Escherichia coli* K-12. Journal of Biological Chemistry. 1982; 257(6):2926–2931.

Ames GFL, Liu CE, Joshi AK, Nikaido K. Liganded and unliganded receptors interact with equal affinity with the membrane complex of periplasmic permeases, a subfamily of traffic ATPases. Journal of Biological Chemistry. 1996; 271(24):14264–14270.

Armenteros JJA, Tsirigos KD, Sønderby CK, Petersen TN, Winther O, Brunak S, von Heijne G, Nielsen H. SignalP 5.0 improves signal peptide predictions using deep neural networks. Nature Biotechnology. 2019; 37(4):420.

Bishop L, Agbayani R, Ambudkar SV, Maloney PC, Ames G. Reconstitution of a bacterial periplasmic permease in proteoliposomes and demonstration of ATP hydrolysis concomitant with transport. Proceedings of the National Academy of Sciences. 1989; 86(18):6953–6957.

de Boer M, Gouridis G, Vietrov R, Begg SL, Schuurman-Wolters GK, Husada F, Eleftheriadis N, Poolman B, McDevitt CA, Cordes T. Conformational and dynamic plasticity in substrate-binding proteins underlies selective transport in ABC importers. Elife. 2019; 8:e44652.

589 **Carlson ML**, Young JW, Zhao Z, Fabre L, Jun D, Li J, Li J, Dhupar HS, Wason I, Mills AT, et al. The Peptidisc, a
590 simple method for stabilizing membrane proteins in detergent-free solution. Elife. 2018; 7:e34085.

591 **Castañeda-Roldán EI**, Ouahrani-Bettache S, Saldaña Z, Avelino F, Rendón MA, Dornand J, Girón JA. Character-
592 ization of SP41, a surface protein of *Brucella* associated with adherence and invasion of host epithelial cells.
593 Cellular Microbiology. 2006; 8(12):1877–1887.

594 **Cockerell SR**, Rutkovsky AC, Zayner JP, Cooper RE, Porter LR, Pendergraft SS, Parker ZM, McGinnis MW, Karatan
595 E. Vibrio cholerae NspS, a homologue of ABC-type periplasmic solute binding proteins, facilitates transduc-
596 tion of polyamine signals independent of their transport. Microbiology. 2014; 160(Pt 5):832.

597 **Consortium U**. UniProt: a worldwide hub of protein knowledge. Nucleic Acids Research. 2019; 47(D1):D506–
598 D515.

599 **Croll TI**. ISOLDE: a physically realistic environment for model building into low-resolution electron-density
600 maps. Acta Crystallographica Section D: Structural Biology. 2018; 74(6):519–530.

601 **Dalvit C**, Fagerness PE, Hadden DT, Sarver RW, Stockman BJ. Fluorine-NMR experiments for high-throughput
602 screening: theoretical aspects, practical considerations, and range of applicability. Journal of the American
603 Chemical Society. 2003; 125(25):7696–7703.

604 **Dalvit C**, Vulpetti A. Ligand-based Fluorine NMR Screening: Principles and Applications in Drug Discovery
605 Projects. Journal of Medicinal Chemistry. 2018; .

606 **Davidson AL**, Shuman HA, Nikaido H. Mechanism of maltose transport in Escherichia coli: transmembrane sig-
607 naling by periplasmic binding proteins. Proceedings of the National Academy of Sciences. 1992; 89(6):2360–
608 2364.

609 **Emsley P**, Lohkamp B, Scott WG, Cowtan K. Features and development of Coot. Acta Crystallographica Section
610 D: Biological Crystallography. 2010; 66(4):486–501.

611 **Fantappiè L**, Irene C, De Santis M, Armini A, Gagliardi A, Tomasi M, Parri M, Cafardi V, Bonomi S, Ganfini L,
612 et al. Some Gram-negative lipoproteins keep their surface topology when transplanted from one species
613 to another and deliver foreign polypeptides to the bacterial surface. Molecular & Cellular Proteomics. 2017;
614 16(7):1348–1364.

615 **Gerber S**, Comellas-Bigler M, Goetz BA, Locher KP. Structural basis of trans-inhibition in a molybdate/tungstate
616 ABC transporter. Science. 2008; 321(5886):246–250.

617 **Gerig J**. Fluorine NMR of proteins. Progress in Nuclear Magnetic Resonance Spectroscopy. 1994; 26:293–370.

618 **Gerlt JA**, Bouvier JT, Davidson DB, Imker HJ, Sadkhin B, Slater DR, Whalen KL. Enzyme function initiative-enzyme
619 similarity tool (EFI-EST): a web tool for generating protein sequence similarity networks. Biochimica Et Bio-
620 physica Acta (BBA)-Proteins and Proteomics. 2015; 1854(8):1019–1037.

621 **Goddard TD**, Huang CC, Meng EC, Pettersen EF, Couch GS, Morris JH, Ferrin TE. UCSF ChimeraX: Meeting
622 modern challenges in visualization and analysis. Protein Science. 2018; 27(1):14–25.

623 **Hantke K**, Braun V. Covalent Binding of Lipid to Protein: Diglyceride and Amide-Linked Fatty Acid at the N-
624 Terminal End of the Murein-Lipoprotein of the *Escherichia coli* Outer Membrane. European Journal of Bio-
625 chemistry. 1973; 34(2):284–296.

626 **Hazelbauer GL**. Maltose chemoreceptor of *Escherichia coli*. Journal of Bacteriology. 1975; 122(1):206–214.

627 **Heppel LA**. The effect of osmotic shock on release of bacterial proteins and on active transport. The Journal
628 of General Physiology. 1969; 54(1):95–113.

629 **Hollenstein K**, Frei DC, Locher KP. Structure of an ABC transporter in complex with its binding protein. Nature.
630 2007; 446(7132):213.

631 **Hooda Y**, Lai CCL, Judd A, Buckwalter CM, Shin HE, Gray-Owen SD, Moraes TF. Slam is an outer membrane
632 protein that is required for the surface display of lipidated virulence factors in *Neisseria*. Nature Microbiology.
633 2016; 1(4):16009.

634 **Hussain M**, Ichihara S, Mizushima S. Mechanism of signal peptide cleavage in the biosynthesis of the major
635 lipoprotein of the *Escherichia coli* outer membrane. Journal of Biological Chemistry. 1982; 257(9):5177–5182.

636 **Johnson E**, Nguyen PT, Yeates TO, Rees DC. Inward facing conformations of the MetNI methionine ABC transporter: Implications for the mechanism of transinhibition. Protein Science. 2012; 21(1):84–96.

638 **Kadaba NS**, Kaiser JT, Johnson E, Lee A, Rees DC. The high-affinity E. coli methionine ABC transporter: structure and allosteric regulation. Science. 2008; 321(5886):250–253.

640 **Kadner RJ**. Transport systems for L-methionine in Escherichia coli. Journal of Bacteriology. 1974; 117(1):232–241.

642 **Kadner RJ**. Transport and utilization of D-methionine and other methionine sources in *Escherichia coli*. Journal of Bacteriology. 1977; 129(1):207–216.

644 **Kaleta C**, Schäuble S, Rinas U, Schuster S. Metabolic costs of amino acid and protein production in *Escherichia coli*. Biotechnology Journal. 2013; 8(9):1105–1114.

646 **Kánová E**, Jiménez-Munguía I, Majerová P, Tkáčová Z, Bhide K, Mertinková P, Pulzová L, Kováč A, Bhide M. Deciphering the interactome of Neisseria meningitidis with human brain microvascular endothelial cells. Frontiers in Microbiology. 2018; 9:2294.

649 **Karla A**, Lively MO, Paetzel M, Dalbey R. The identification of residues that control signal peptidase cleavage fidelity and substrate specificity. Journal of Biological Chemistry. 2005; 280(8):6731–6741.

651 **Krismer B**, Liebeke M, Janek D, Nega M, Rautenberg M, Hornig G, Unger C, Weidenmaier C, Lalk M, Peschel A. Nutrient limitation governs *Staphylococcus aureus* metabolism and niche adaptation in the human nose. PLoS Pathog. 2014; 10(1):e1003862.

654 **Krissinel E**, Henrick K. Secondary-structure matching (SSM), a new tool for fast protein structure alignment in three dimensions. Acta Crystallographica Section D: Biological Crystallography. 2004; 60(12):2256–2268.

656 **Kwok Y**, Sung WC, Lin ALH, Liu HH, Chou FAH, Hsieh SSY, Leng CH, Chong P. Rapid isolation and characterization of bacterial lipopeptides using liquid chromatography and mass spectrometry analysis. Proteomics. 2011; 11(13):2620–2627.

659 **Lee KJ**, Lee NY, Han YS, Kim J, Lee KH, Park SJ. Functional characterization of the IlpA protein of *Vibrio vulnificus* as an adhesin and its role in bacterial pathogenesis. Infection and Immunity. 2010; 78(6):2408–2417.

661 **Liu F**, Liang J, Zhang B, Gao Y, Yang X, Hu T, Yang H, Xu W, Guddat LW, Rao Z. Structural basis of trehalose recycling by the ABC transporter LpqY-SugABC. Science advances. 2020; 6(44):eabb9833.

663 **Locher KP**, Lee AT, Rees DC. The *E. coli* BtuCD structure: a framework for ABC transporter architecture and mechanism. Science. 2002; 296(5570):1091–1098.

665 **Luo Y**, Friese OV, Runnels HA, Khandke L, Zlotnick G, Aulabaugh A, Gore T, Vidunas E, Raso SW, Novikova E, et al. The dual role of lipids of the lipoproteins in trumenba, a self-adjuvanting vaccine against meningococcal meningitis B disease. The AAPS journal. 2016; 18(6):1562–1575.

668 **Manson MD**, Boos W, Bassford Jr P, Rasmussen B. Dependence of maltose transport and chemotaxis on the amount of maltose-binding protein. Journal of Biological Chemistry. 1985; 260(17):9727–9733.

670 **Mao G**, Zhao Y, Kang X, Li Z, Zhang Y, Wang X, Sun F, Sankaran K, Zhang XC. Crystal structure of *E. coli* lipoprotein diacylglyceryl transferase. Nature Communications. 2016; 7(1):1–12.

672 **Mastronarde DN**. Automated electron microscope tomography using robust prediction of specimen movements. Journal of Structural Biology. 2005; 152(1):36–51.

674 **Matthysse AG**, Yarnall HA, Young N. Requirement for genes with homology to ABC transport systems for attachment and virulence of *Agrobacterium tumefaciens*. Journal of Bacteriology. 1996; 178(17):5302–5308.

676 **Mimmack M**, Gallagher M, Pearce S, Hyde S, Booth I, Higgins C. Energy coupling to periplasmic binding protein-dependent transport systems: stoichiometry of ATP hydrolysis during transport *in vivo*. Proceedings of the National Academy of Sciences. 1989; 86(21):8257–8261.

679 **Müller A**, León-Kempis MdR, Dodson E, Wilson KS, Wilkinson AJ, Kelly DJ. A bacterial virulence factor with a dual role as an adhesin and a solute-binding protein: the crystal structure at 1.5 Å resolution of the PEB1a protein from the food-borne human pathogen *Campylobacter jejuni*. Journal of molecular biology. 2007; 372(1):160–171.

683 **Nguyen PT**, Lai JY, Kaiser JT, Rees DC. Structures of the *Neisseria meningitides* methionine-binding protein MetQ
684 in substrate-free form and bound to l-and d-methionine isomers. Protein Science. 2019; 28(10):1750–1757.

685 **Nguyen PT**, Lai JY, Lee AT, Kaiser JT, Rees DC. Noncanonical role for the binding protein in substrate uptake
686 by the MetNI methionine ATP Binding Cassette (ABC) transporter. Proceedings of the National Academy of
687 Sciences. 2018; 115(45):E10596–E10604.

688 **Nguyen PT**, Li QW, Kadaba NS, Lai JY, Yang JG, Rees DC. The contribution of methionine to the stability of
689 the Escherichia coli MetNIQ ABC transporter-substrate binding protein complex. Biological chemistry. 2015;
690 396(9-10):1127–1134.

691 **Noland CL**, Kattke MD, Diao J, Gloor SL, Pantua H, Reichelt M, Katakam AK, Yan D, Kang J, Zilberleyb I, et al. Struc-
692 tural insights into lipoprotein N-acylation by *Escherichia coli* apolipoprotein N-acyltransferase. Proceedings
693 of the National Academy of Sciences. 2017; 114(30):E6044–E6053.

694 **Okuda S**, Tokuda H. Lipoprotein sorting in bacteria. Annual review of microbiology. 2011; 65:239–259.

695 **Oldham ML**, Chen S, Chen J. Structural basis for substrate specificity in the *Escherichia coli* maltose transport
696 system. Proceedings of the National Academy of Sciences. 2013; 110(45):18132–18137.

697 **Paetzel M**, Dalbey RE, Strynadka NC. Crystal structure of a bacterial signal peptidase in complex with a β-lactam
698 inhibitor. Nature. 1998; 396(6707):186–190.

699 **Parra MC**, Shaffer SA, Hajjar AM, Gallis BM, Hager A, Goodlett DR, Guina T, Miller S, Collins CM. Identifica-
700 tion, cloning, expression, and purification of Francisella lpp3: an immunogenic lipoprotein. Microbiological
701 Research. 2010; 165(7):531–545.

702 **Pettersen EF**, Goddard TD, Huang CC, Meng EC, Couch GS, Croll TI, Morris JH, Ferrin TE. UCSF ChimeraX: Struc-
703 ture visualization for researchers, educators, and developers. Protein Science. 2021; 30(1):70–82.

704 **Pinkett H**, Lee A, Lum P, Locher K, Rees D. An inward-facing conformation of a putative metal-chelate-type
705 ABC transporter. Science. 2007; 315(5810):373–377.

706 **Pizza M**, Scarlato V, Masignani V, Giuliani MM, Arico B, Comanducci M, Jennings GT, Baldi L, Bartolini E, Capecchi
707 B, et al. Identification of vaccine candidates against serogroup B meningococcus by whole-genome sequenc-
708 ing. Science. 2000; 287(5459):1816–1820.

709 **Punjani A**, Rubinstein JL, Fleet DJ, Brubaker MA. cryoSPARC: algorithms for rapid unsupervised cryo-EM struc-
710 ture determination. Nature Methods. 2017; 14(3):290–296.

711 **Sabrialabed S**, Yang JG, Yariv E, Ben-Tal N, Lewinson O. Substrate recognition and ATPase activity of the *E. coli*
712 cysteine/cystine ABC transporter YecSC-FliY. Journal of Biological Chemistry. 2020; 295(16):5245–5256.

713 **Schmidt A**, Kochanowski K, Vedelaar S, Ahrné E, Volkmer B, Callipo L, Knoops K, Bauer M, Aebersold R, Heine-
714 mann M. The quantitative and condition-dependent *Escherichia coli* proteome. Nature biotechnology. 2016;
715 34(1):104–110.

716 **Semchenko EA**, Day CJ, Seib KL. MetQ of *Neisseria gonorrhoeae* is a surface expressed antigen that elicits
717 bactericidal and functional blocking antibodies. Infection and Immunity. 2016; p. IAI–00898.

718 **Smith T**, Ghandour MS, Wood PL. Detection of N-acetyl methionine in human and murine brain and neuronal
719 and glial derived cell lines. Journal of Neurochemistry. 2011; 118(2):187–194.

720 **Smoot ME**, Ono K, Ruscheinski J, Wang PL, Ideker T. Cytoscape 2.8: new features for data integration and
721 network visualization. Bioinformatics. 2011; 27(3):431–432.

722 **Stephens DS**, Greenwood B, Brandtzaeg P. Epidemic meningitis, meningococcaemia, and *Neisseria meningitidis*.
723 The Lancet. 2007; 369(9580):2196–2210.

724 **Studier FW**. Protein production by auto-induction in high-density shaking cultures. Protein Expression and
725 Purification. 2005; 41(1):207–234.

726 **Thomas C**, Tampé R. Structural and Mechanistic Principles of ABC Transporters. Annual Review of Biochemistry.
727 2020; 89:605–636.

728 **Tokuda H**, Matsuyama Si, Tanaka-Masuda K. Structure, function, and transport of lipoproteins in *Escherichia*
729 *coli*. In: *The Periplasm* American Society of Microbiology; 2007.p. 67–79.

730 **Vogeley L**, El Arnaout T, Bailey J, Stansfeld PJ, Boland C, Caffrey M. Structural basis of lipoprotein signal peptidase II action and inhibition by the antibiotic globomycin. Science. 2016; 351(6275):876–880.

732 **Wiktor M**, Weichert D, Howe N, Huang CY, Olieric V, Boland C, Bailey J, Vogeley L, Stansfeld PJ, Buddelmeijer N, et al. Structural insights into the mechanism of the membrane integral N-acyltransferase step in bacterial lipoprotein synthesis. Nature communications. 2017; 8(1):1–13.

735 **Willis RC**, Furlong CE. Purification and properties of a ribose-binding protein from *Escherichia coli*. Journal of Biological Chemistry. 1974; 249(21):6926–6929.

737 **Young EC**, Baumgartner JT, Karatan E, Kuhn ML. A mutagenic screen reveals NspS residues important for regulation of *Vibrio cholerae* biofilm formation. Microbiology. 2021; p. 001023.

739 **Yu S**, Lee NY, Park SJ, Rhee S. Crystal structure of toll-like receptor 2-activating lipoprotein IIpA from *Vibrio vulnificus*. Proteins: structure, Function, and Bioinformatics. 2011; 79(3):1020–1025.

741 **Zückert WR**. Secretion of bacterial lipoproteins: through the cytoplasmic membrane, the periplasm and beyond. Biochimica et Biophysica Acta (BBA)-Molecular Cell Research. 2014; 1843(8):1509–1516.

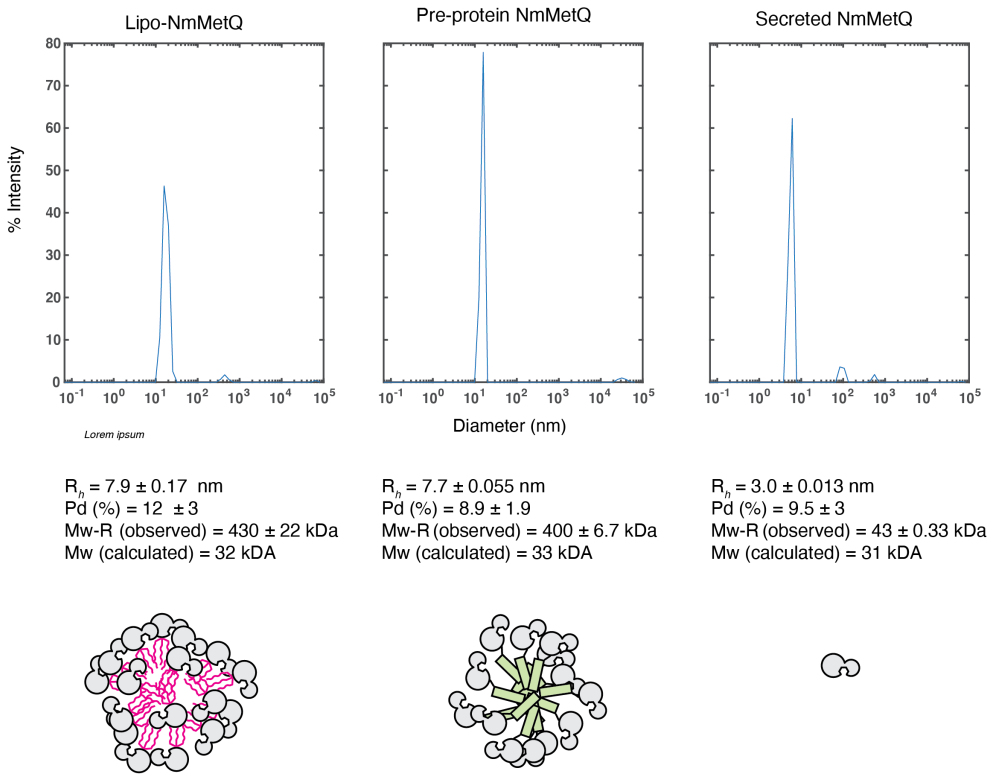

743

Figure 1–Figure supplement 1. DLS measurement of NmMetQ proteins. Representative DLS intensity distribution plots of lipo-NmmetQ (0.7 mg/ml), pre-protein (2.3 mg/ml) and secreted NmMetQ (2.7 mg/ml) (top panel). The hydrodynamic radius (R_h), the polydispersity (Pd %), molecular weight estimate based on the hydrodynamic radius of a folded globular protein (Mw-R) are listed below each plot. The mean and SEM of each measurement were calculated from triplicate measurements. Proposed models of NmMetQ protein quaternary arrangements (bottom panel)

	Inward facing conformation of the MetNI methionine ABC transporter	Outward facing conformation of the MetNI methionine ABC transporter in complex with lipo-MetQ
PDB	**7MC0**	**7MBZ**
EMD	**EMD-23752**	**EMD-23751**
Data collection conditions		
Microscope	Titan Krios	Titan Krios
Camera	Gatan K3 Summit	Gatan K3 Summit
Magnification	105,000x	105,000x
Voltage (kV)	300	300
Recording mode	counting	counting
Frames/Movies	40	40
Total Electron dose ($e^-/Å^2$)	60	60
Defocus range (μm)	1.0 – 2.8	1.0-2.8
Pixel size (Å)	0.856	0.856
Micrographs collected	4,709	6,183
Micrographs used	3,968	5,494
Total extracted particles	1,684,719	2,874,862
Refined particles	322,171	58,434
Symmetry imposed	C1	C1
Nominal Map Resolution (Å)		
FSC 0.143 (unmasked/masked)	3.4/3.3	6.4/6.4
Refinement and Validation		
Initial model used	3TUJ	
Number of atoms		
Protein	7,092	8,987
Ligand	0	0
MapCC (mask/box)	0.80/0.65	0.75/0.69
Map sharpening B-factor	91.3	496
R.m.s. deviations		
Bond lengths (Å)	0.012	0.012
Bond angles (°)	1.62	1.92
MolProbity score	1.76	1.73
Clashscore (all atom)	7.56	6.77
Rotamer outliers (%)	1.19	1.04
Ramachandran plot		
Favored (%)	95.77	95.09
Allowed (%)	3.90	4.91
Outliers (%)	0.33	0

Figure 4–Figure supplement 1. CryoEM data collection and refinement statistics.

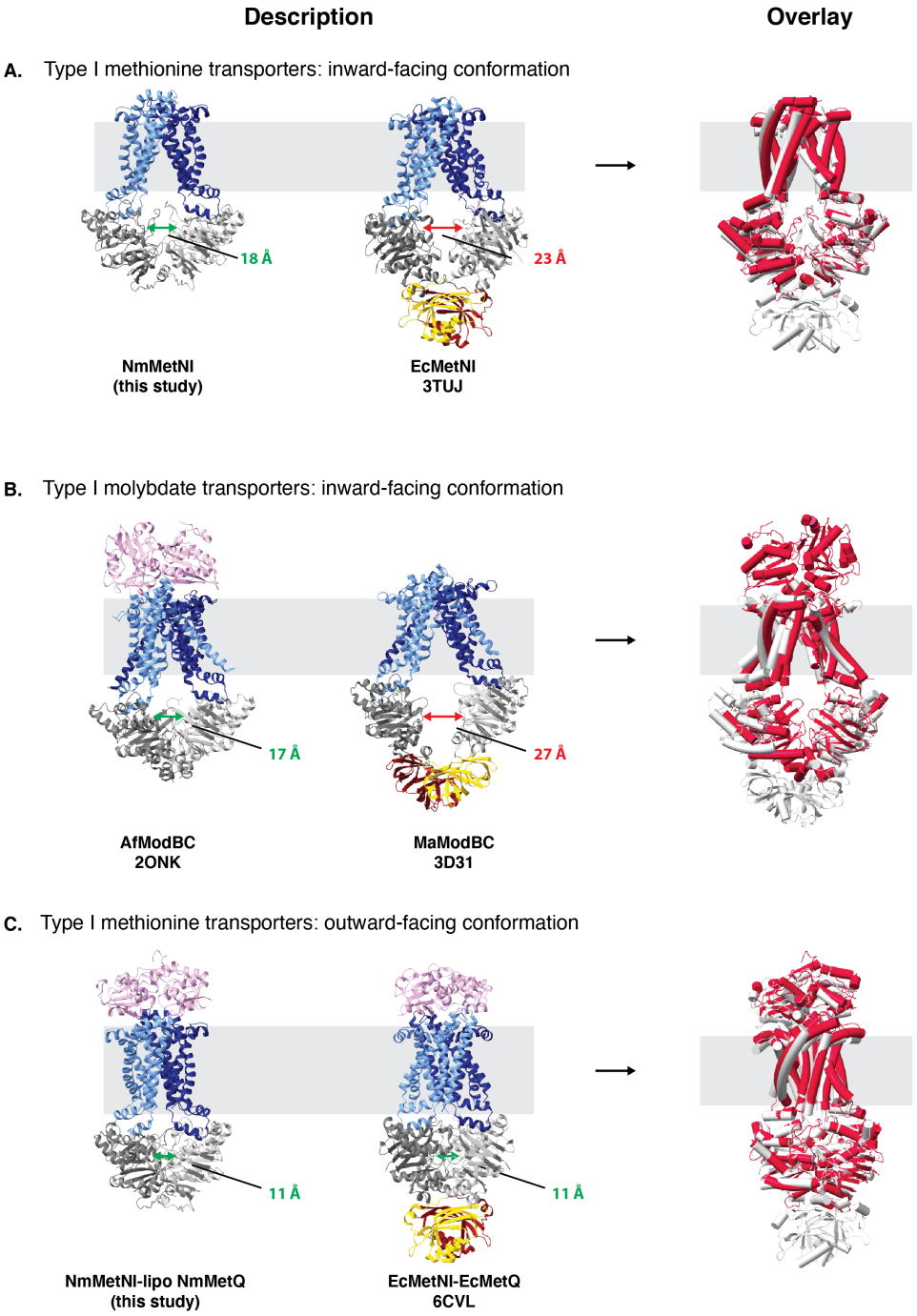

Figure 4–Figure supplement 2. Comparison of type I ABC transporters. A. ABC methionine transporters in the inward-facing conformation. B ABC molybdate transporters in the inward-facing conformation and C. ABC methionine transporters in the outward-facing conformation. For each model the TMDs,NBDs and SBPs, are colored in blue, grey, and pink, respectively. Next to each panel, an overlay is included of the two structures, with the ABC transporter with a regulatory domain colored in grey and the ABC transporter with a regulatory domain colored in red. NBD:NBD inter-subunit distances were assessed using the Cα of NBD glycine residues in the P loop and signature motifs. The average of the two distances are indicated by double arrows.

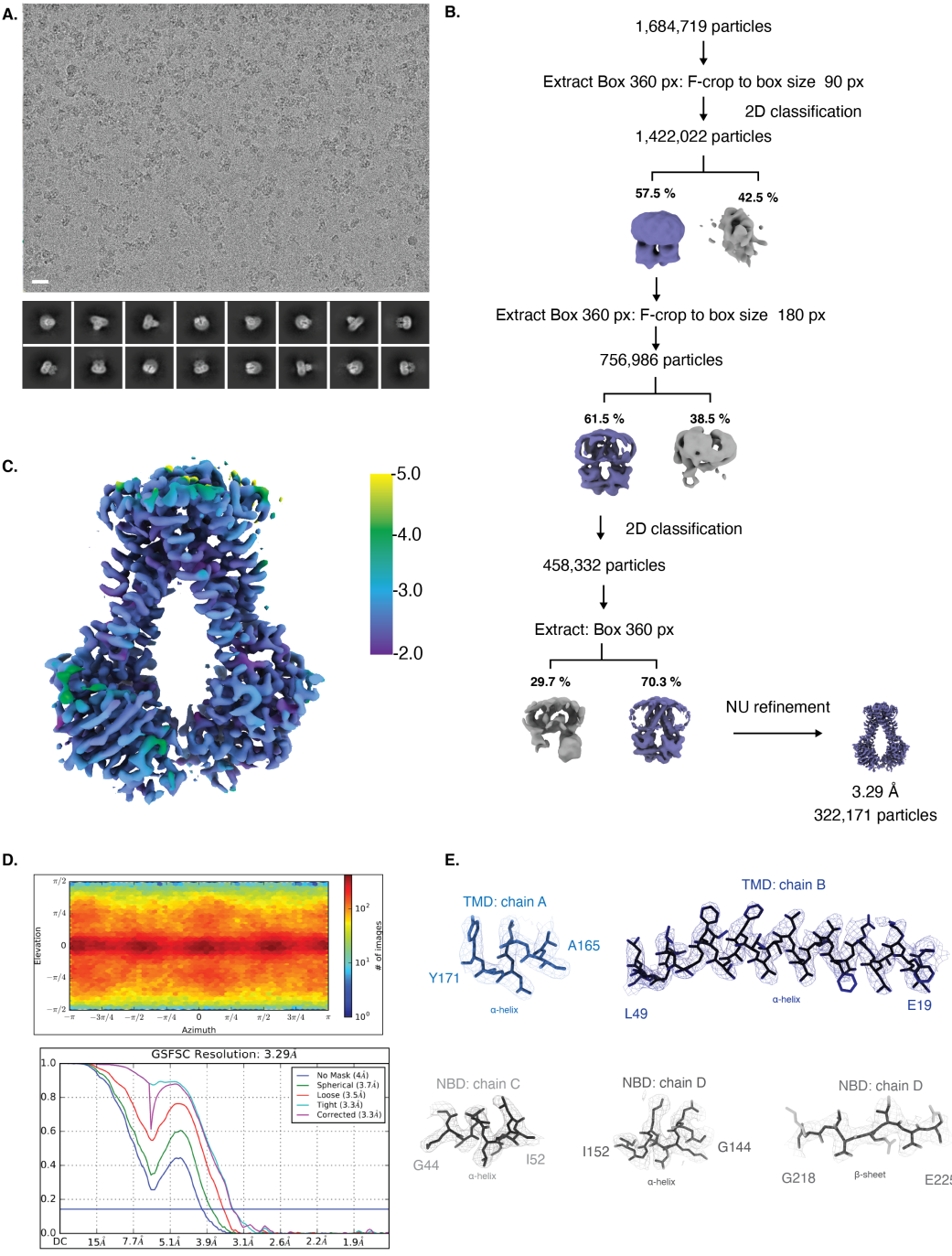

Figure 4–Figure supplement 3. CryoEM map generation and data processing refinement of NmMetNI in the inward-facing conformation. A. Representative cryoEM micrograph of (scale bar is 20 nm) and select 2D class averages. B. Workflow of single-particle image processing. C. Local resolution plot of NmMetNI as calculated using cryoSPARC. D. Angular distribution calculated for particle projections. Heatmap shows number of particles for each viewing angle (top) and gold-standard Fourier shell correlation (FSC) curves for masked and unmasked maps generated by cryoSPARC non-uniform refinement (bottom) E. CryoEM density (mesh) overlaid on the atomic model of select regions of NmMetNI. (sticks).

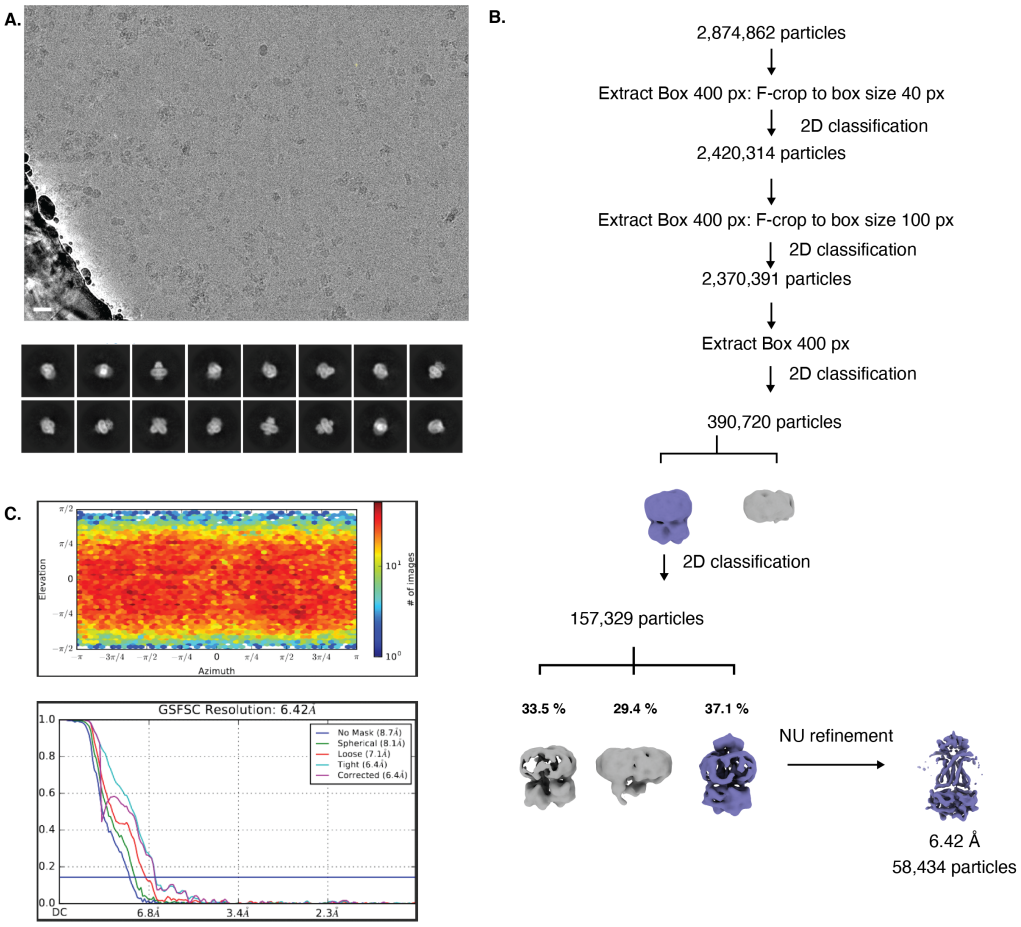

747

Figure 4–Figure supplement 4. CryoEM map generation and data processing refinement of lipo-NmMetQ:NmMetNI complex in the outward-facing conformation. A. Representative cryoEM micrograph of (scale bar is 20 nm) and select 2D class averages. B. Workflow of single-particle image processing. C. Angular distribution calculated for particle projections. Heatmap shows number of particles for each viewing angle (top) and gold-standard Fourier shell correlation (FSC) curves for masked and unmasked maps generated by cryoSPARC non-uniform refinement (bottom).

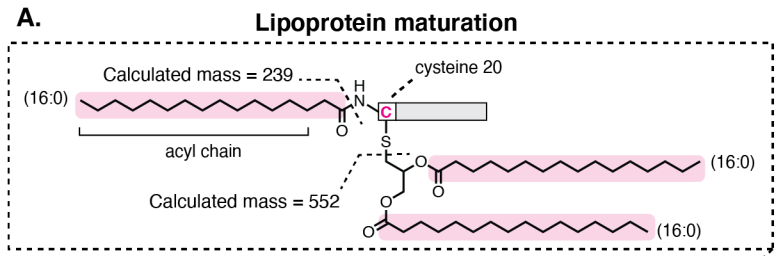

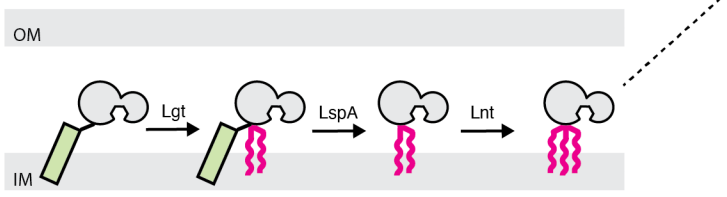

Theoretical masses for lipo-NmMetQ proteins

Pre-prolipoprotein	Prolipoprotein	Diacylated lipoprotein	Triacylated lipoprotein
32,834	*33,385* [16:0, 16:0]	*31,421* [16:0, 16:0]	*31,660* [16:0, 16:0, 16:0]
	33,407 [16:0, 18:1]	*31,443* [16:0, 18:1]	*31,685* [16:0, 18:1, 16:0]

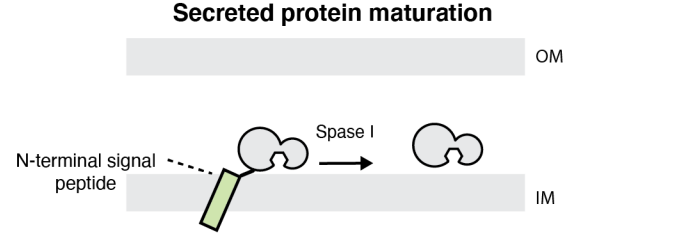

Theoretical masses for NmMetQC20A proteins

Pre-protein	secreted protein
32,802	*30,839*

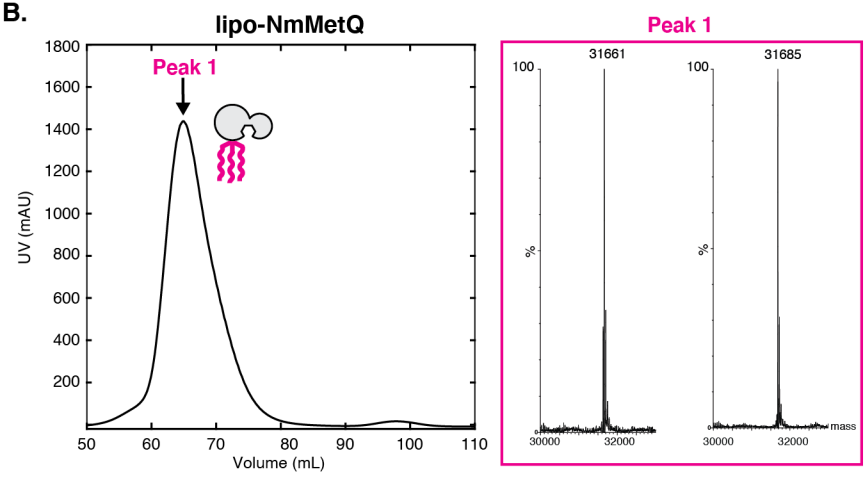

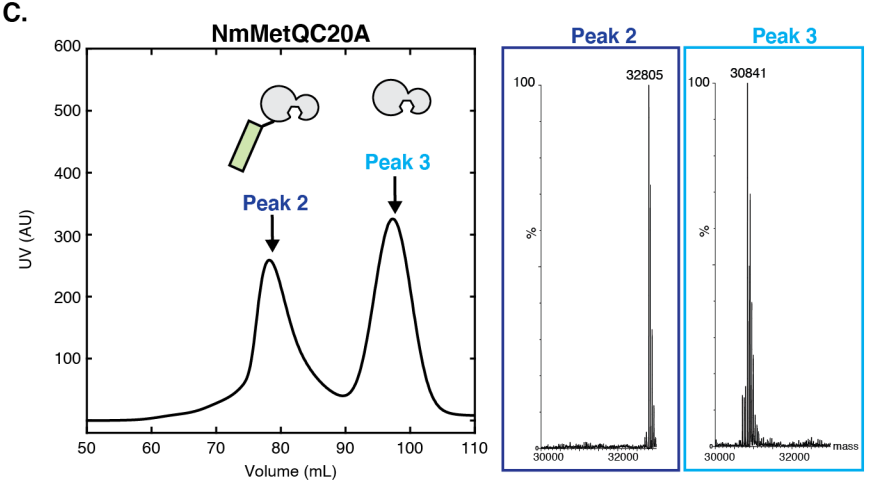

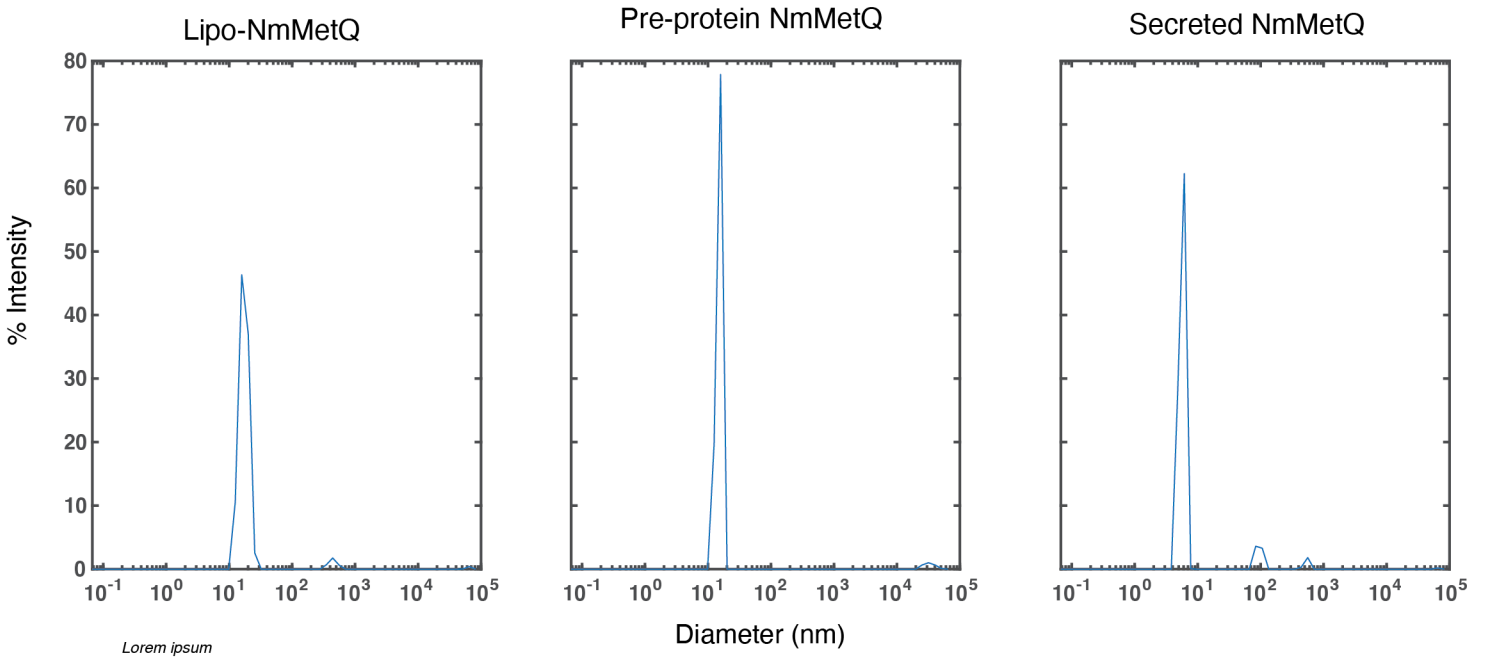

R_h = 7.9 ± 0.17 nm
Pd (%) = 12 ± 3
Mw-R (observed) = 430 ± 22 kDa
Mw (calculated) = 32 kDA

R_h = 7.7 ± 0.055 nm
Pd (%) = 8.9 ± 1.9
Mw-R (observed) = 400 ± 6.7 kDa
Mw (calculated) = 33 kDA

R_h = 3.0 ± 0.013 nm
Pd (%) = 9.5 ± 3
Mw-R (observed) = 43 ± 0.33 kDa
Mw (calculated) = 31 kDA

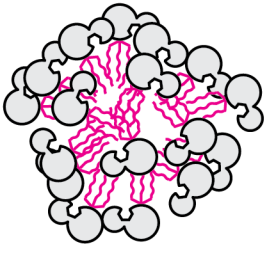

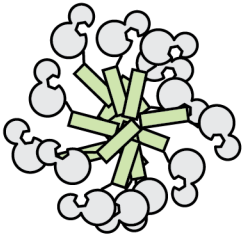

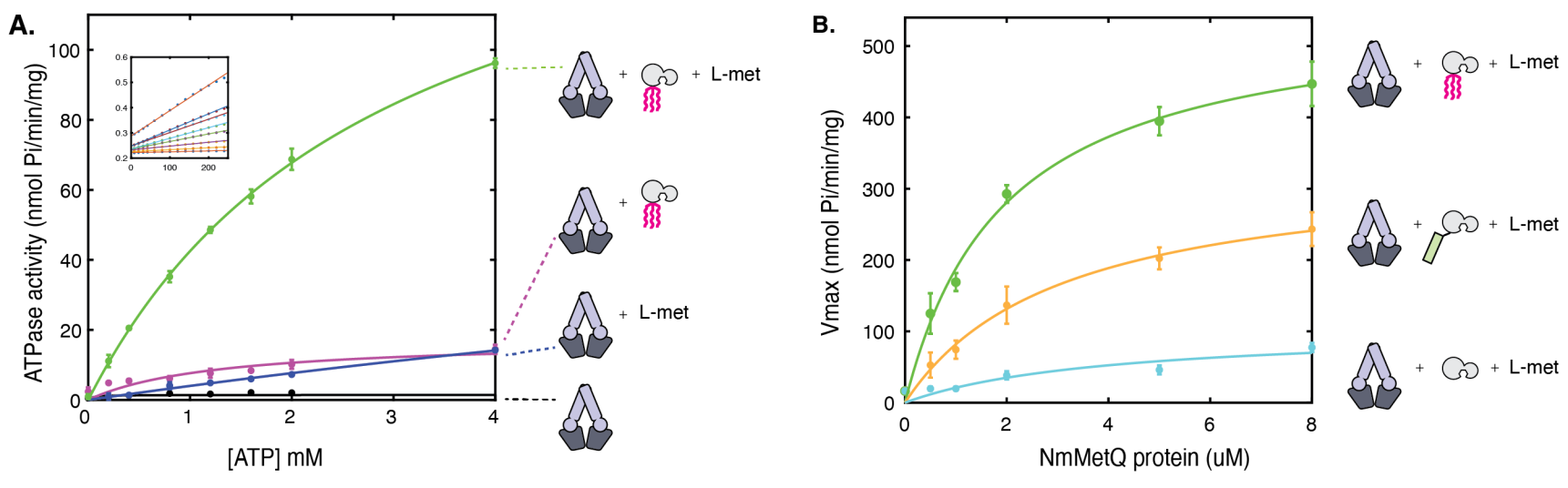
A.
ATPase activity (nmol Pi/min/mg)
[ATP] mM
+ L-met
+ L-met
B.
Vmax (nmol Pi/min/mg)
NmMetQ protein (uM)
+ L-met
+ L-met
+ L-met

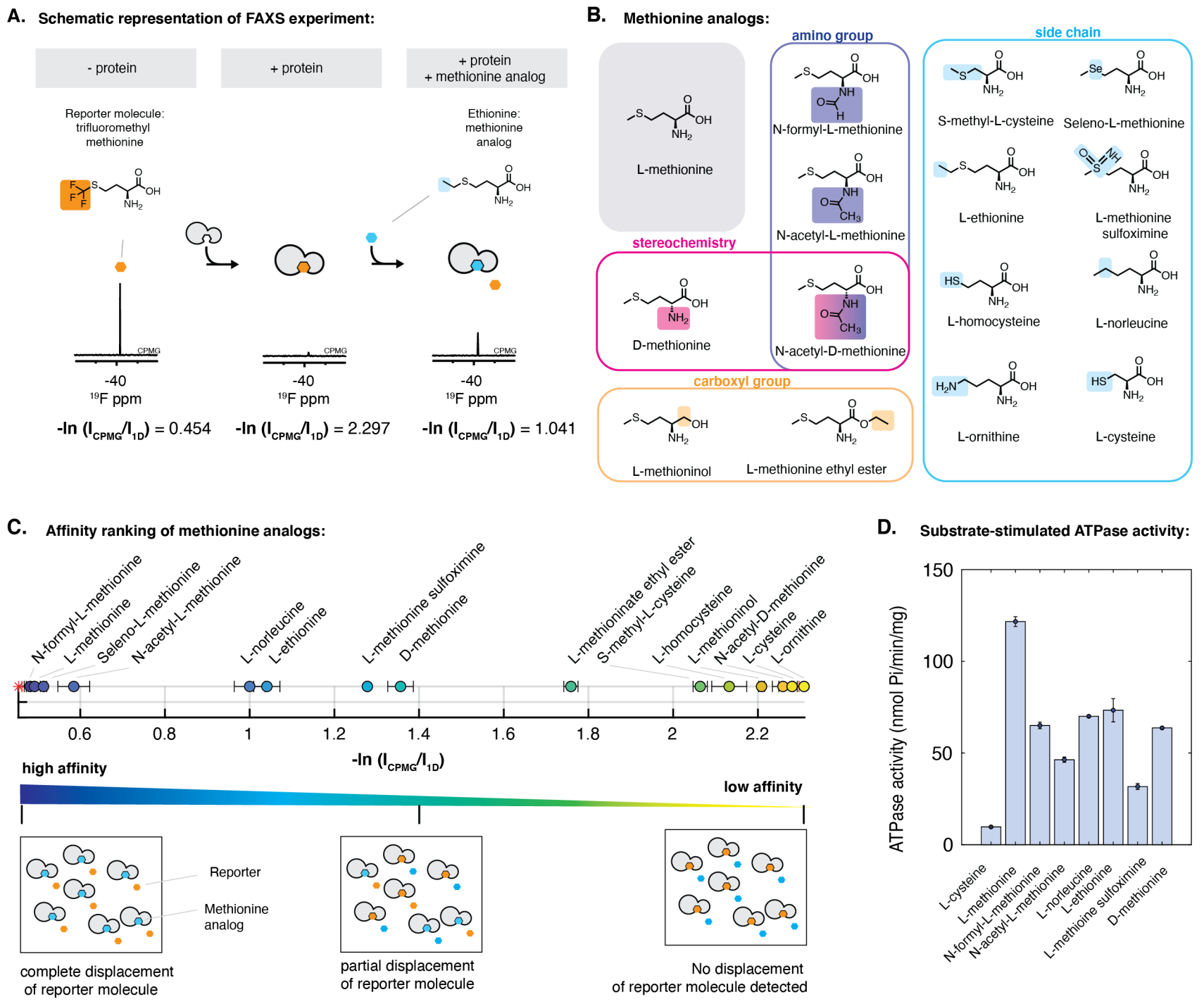
A. Schematic representation of FAXS experiment:
- protein
+ protein
+ protein
+ methionine analog
Reporter molecule: trifluoromethyl methionine
Ethionine: methionine analog
CPMG
-40
19F ppm
-ln (ICPMG/I1D) = 0.454
-ln (ICPMG/I1D) = 2.297
-ln (ICPMG/I1D) = 1.041
B. Methionine analogs:
amino group
side chain
L-methionine
N-formyl-L-methionine
N-acetyl-L-methionine
S-methyl-L-cysteine
Seleno-L-methionine
stereochemistry
L-ethionine
L-methionine sulfoximine
D-methionine
N-acetyl-D-methionine
L-homocysteine
L-norleucine
carboxyl group
L-ornithine
L-cysteine
L-methioninol
L-methionine ethyl ester
C. Affinity ranking of methionine analogs:
N-formyl-L-methionine
L-methionine
Seleno-L-methionine
N-acetyl-L-methionine
L-norleucine
L-ethionine
L-methionine sulfoximine
D-methionine
L-methioninate ethyl ester
S-methyl-L-cysteine
L-homocysteine
L-methioninol
N-acetyl-D-methionine
L-cysteine
L-ornithine
0.6
0.8
1
1.2
1.4
1.6
1.8
2
2.2
-ln (ICPMG/I1D)
high affinity
low affinity
Reporter
Methionine analog
complete displacement of reporter molecule
partial displacement of reporter molecule
No displacement of reporter molecule detected
D. Substrate-stimulated ATPase activity:
ATPase activity (nmol Pi/min/mg)
150
100
50
0
L-cysteine
L-methionine
N-formyl-L-methionine
N-acetyl-L-methionine
L-norleucine
L-ethionine
L-methioine sulfoximine
D-methionine

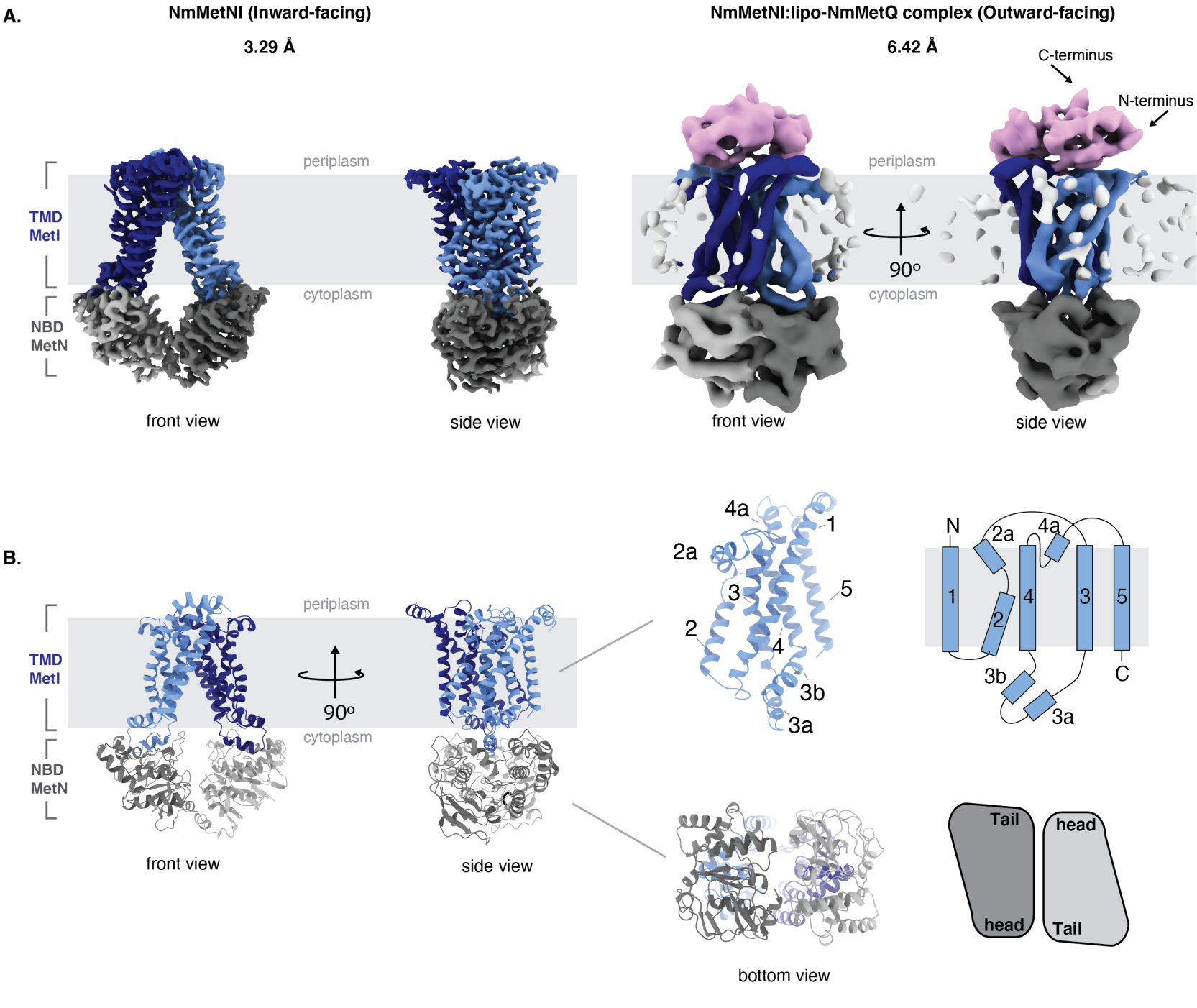
A.
NmMetNI (Inward-facing)
3.29 Å
NmMetNI:lipo-NmMetQ complex (Outward-facing)
6.42 Å
C-terminus
N-terminus
periplasm
cytoplasm
TMD
MetI
NBD
MetN
90°
front view
side view
front view
side view
B.
periplasm
cytoplasm
TMD
MetI
NBD
MetN
90°
front view
side view
4a
1
2a
3
5
2
4
3b
3a
N
2a
4a
1
2
4
3
5
3b
C
3a
bottom view
Tail
head
head
Tail

A.

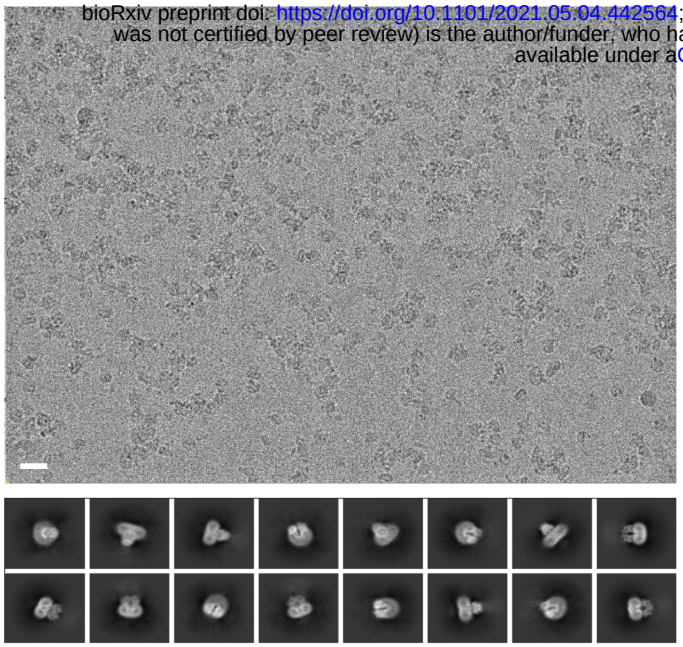

B.

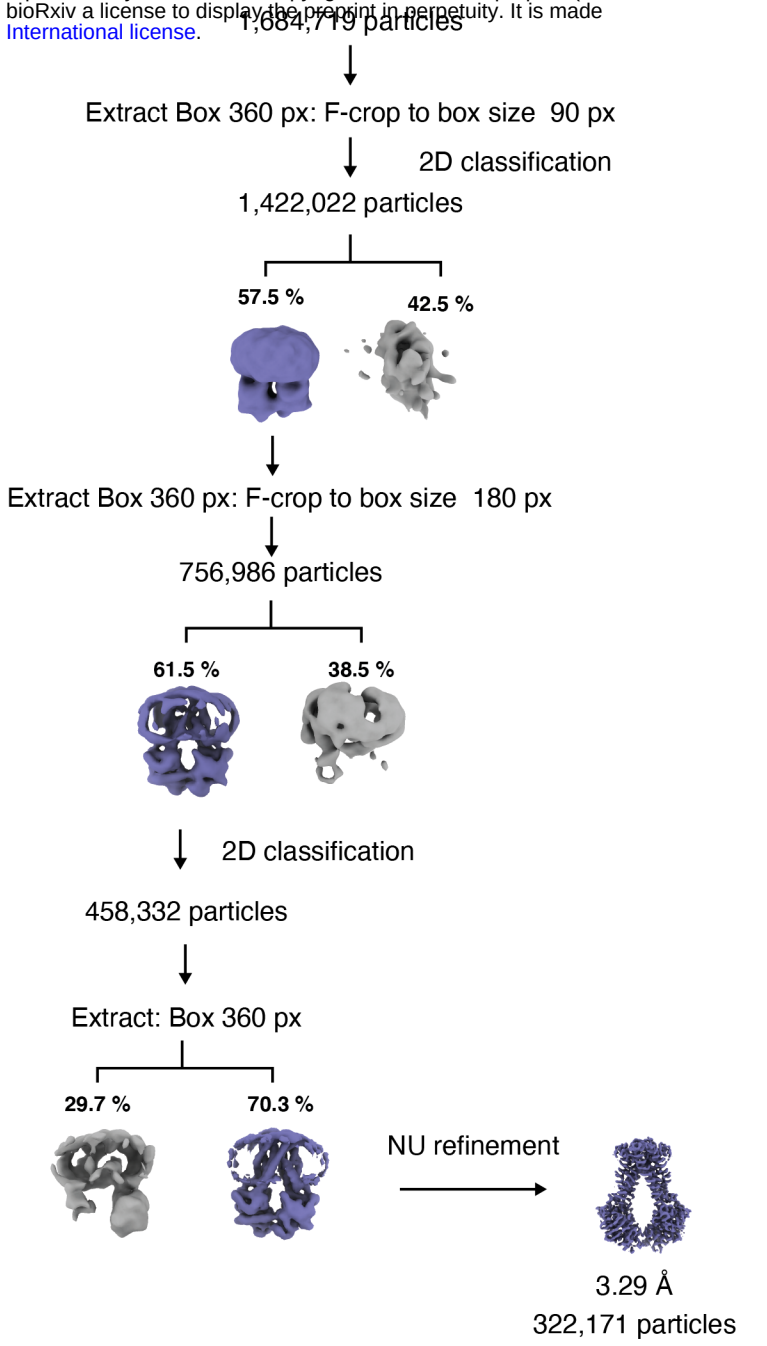

C.

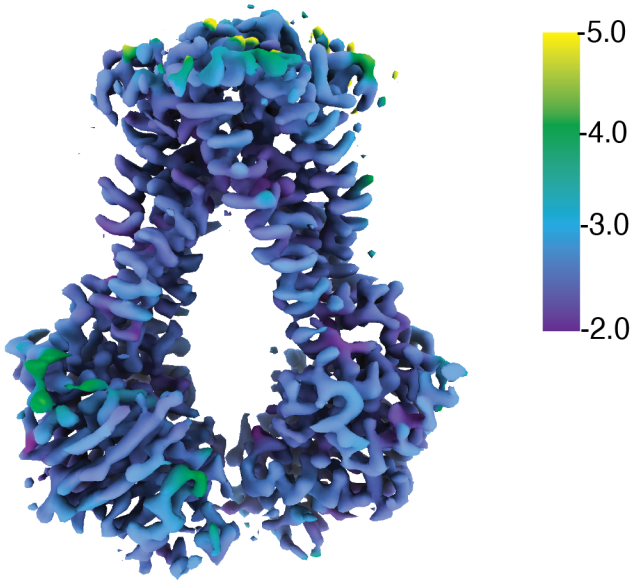

D.

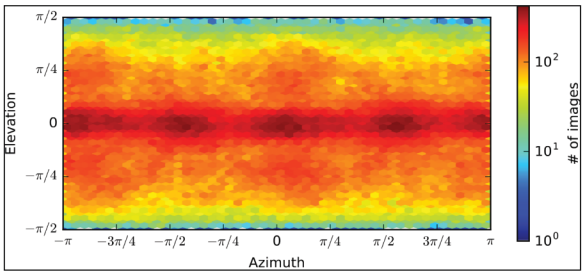

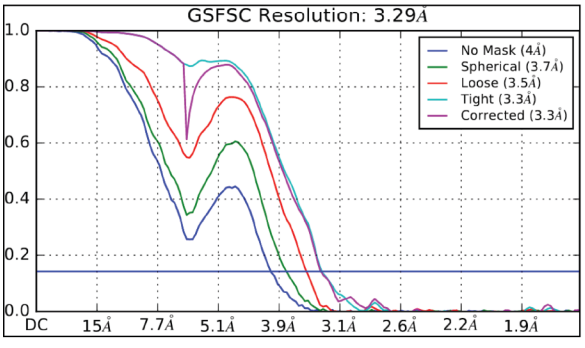

E.

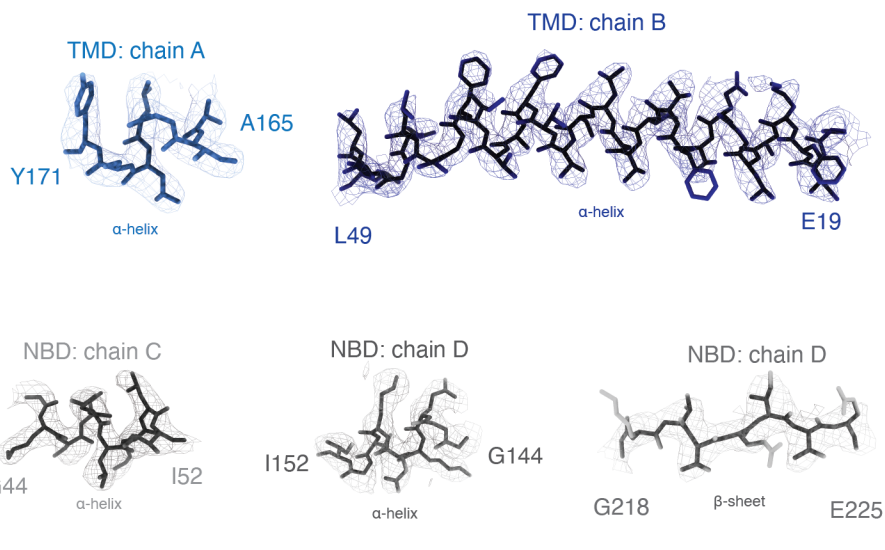

A.

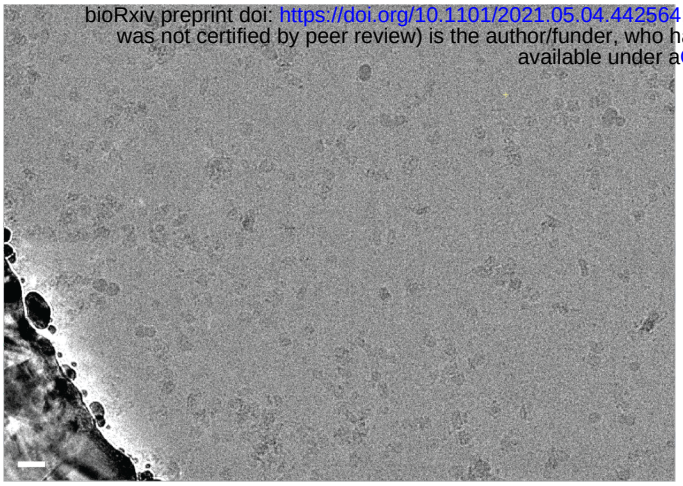

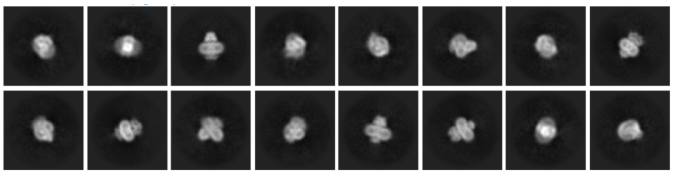

B.

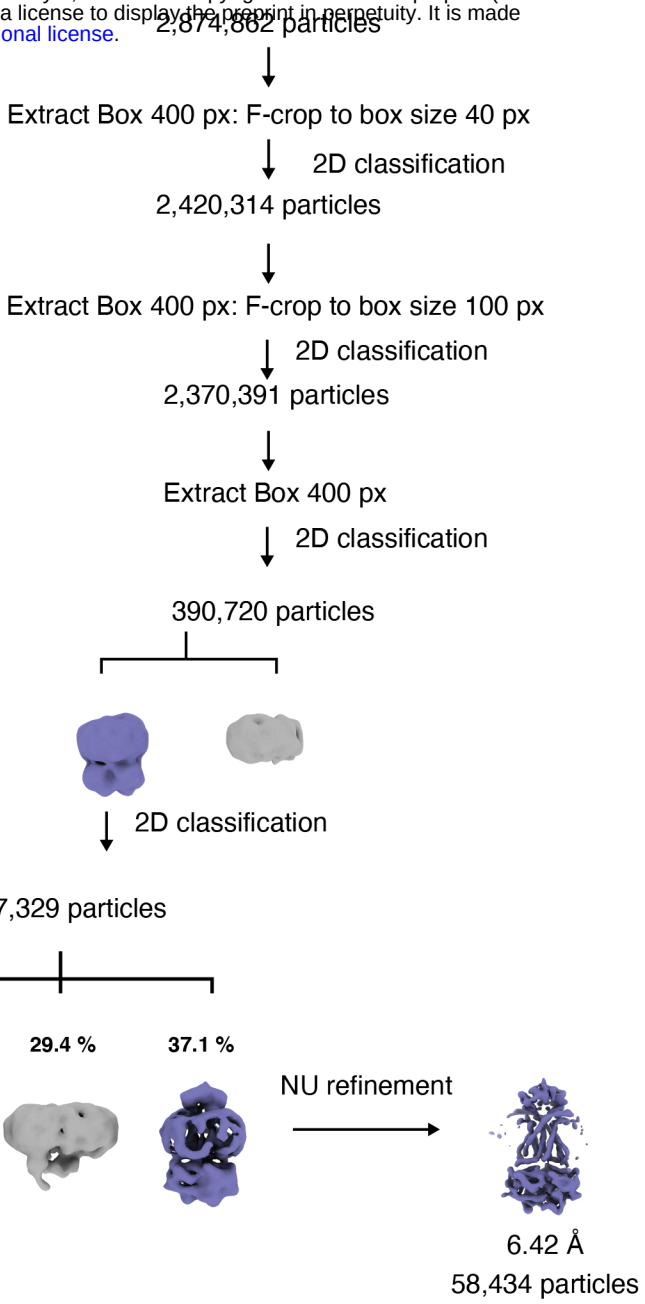

C.

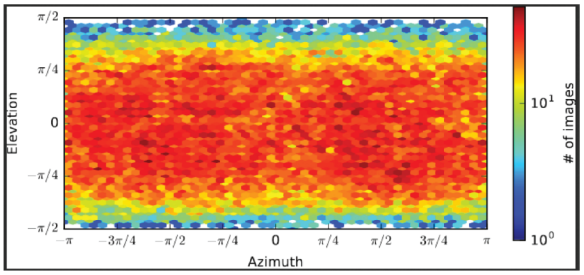

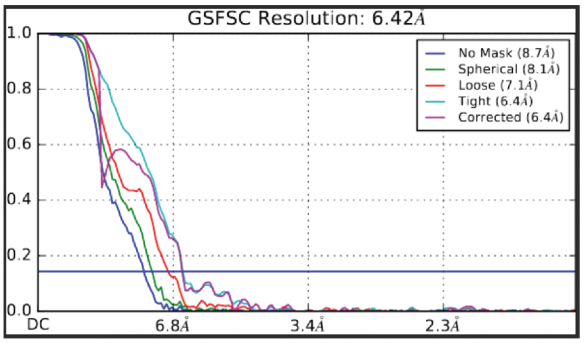

A. Type I methionine transporters: inward-facing conformation

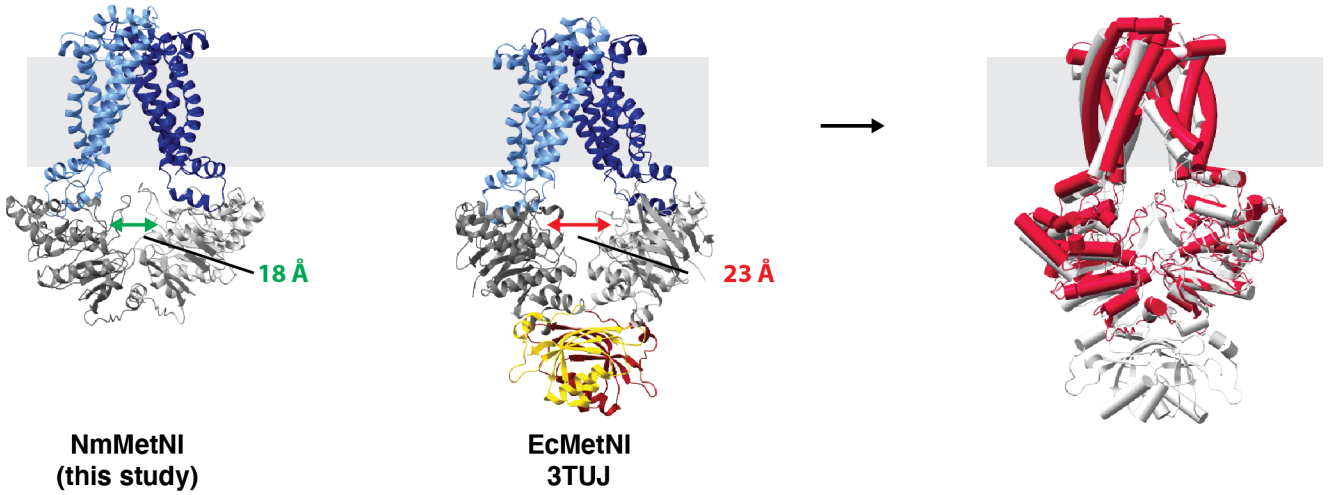

NmMetNI (this study) **EcMetNI 3TUJ**

B. Type I molybdate transporters: inward-facing conformation

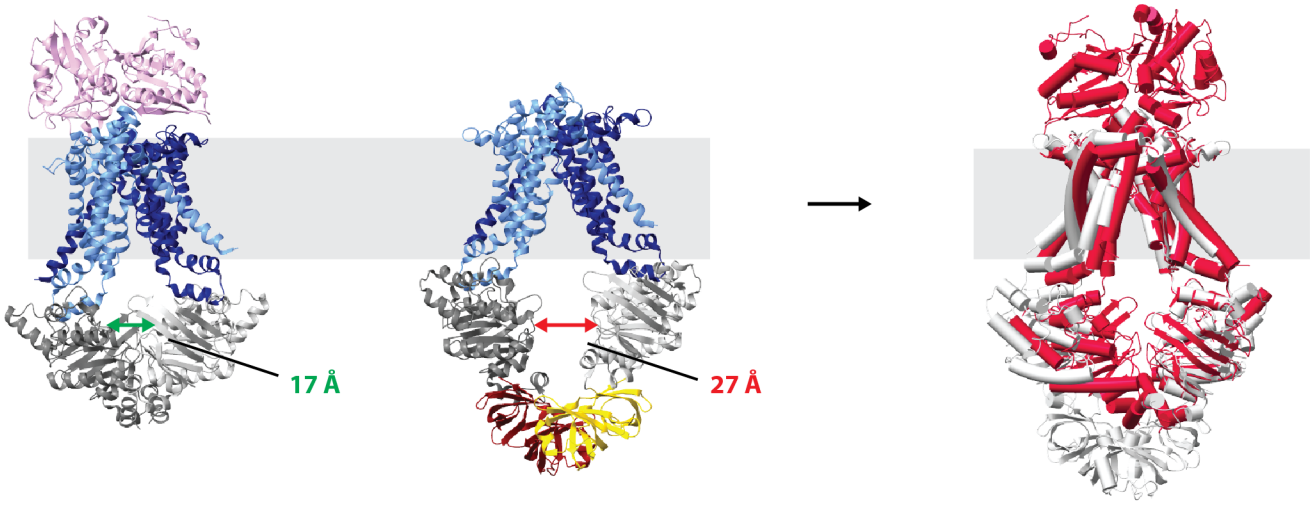

AfModBC 2ONK **MaModBC 3D31**

C. Type I methionine transporters: outward-facing conformation

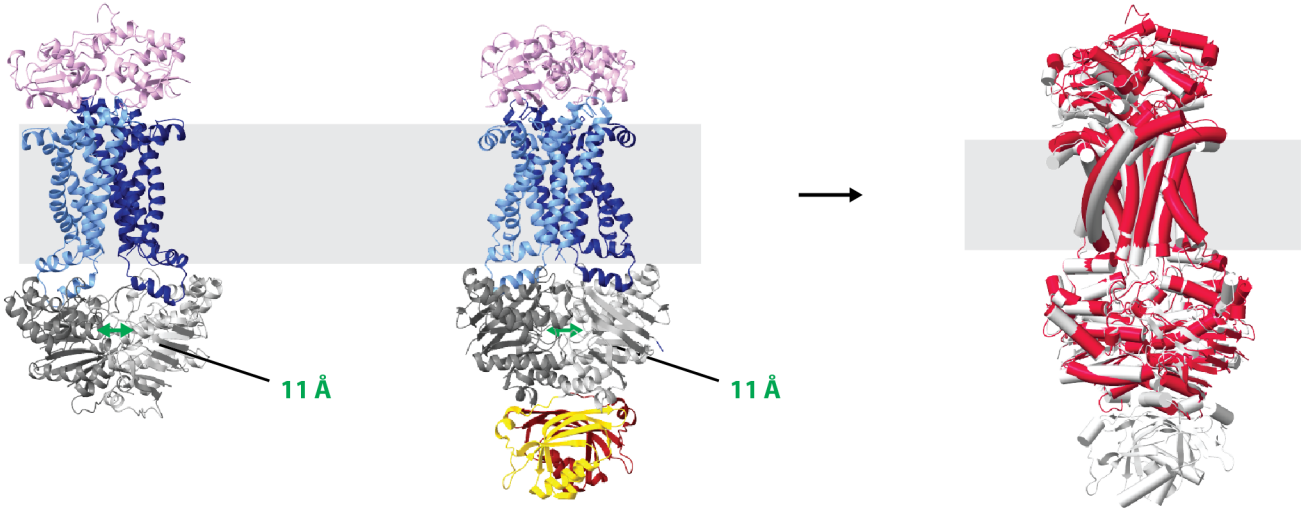

NmMetNI-lipo NmMetQ (this study) **EcMetNI-EcMetQ 6CVL**

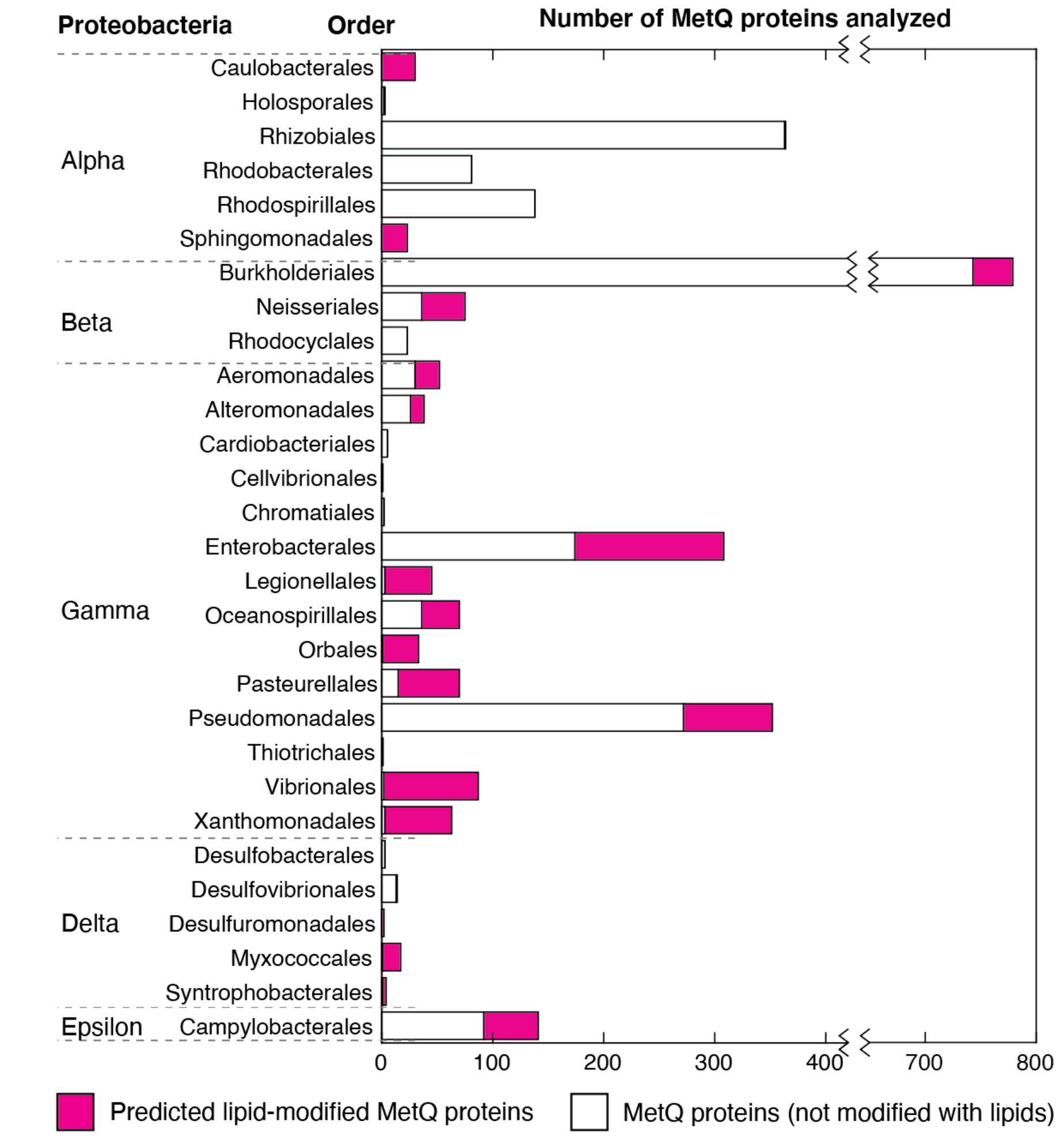
Proteobacteria
Order
Number of MetQ proteins analyzed
Alpha
Caulobacterales
Holosporales
Rhizobiales
Rhodobacterales
Rhodospirillales
Sphingomonadales
Beta
Burkholderiales
Neisseriales
Rhodocyclales
Gamma
Aeromonadales
Alteromonadales
Cardiobacteriales
Cellvibrionales
Chromatiales
Enterobacterales
Legionellales
Oceanospirillales
Orbales
Pasteurellales
Pseudomonadales
Thiotrichales
Vibrionales
Xanthomonadales
Delta
Desulfobacterales
Desulfovibrionales
Desulfuromonadales
Myxococcales
Syntrophobacterales
Epsilon
Campylobacterales
0
100
200
300
400
700
800
Predicted lipid-modified MetQ proteins
MetQ proteins (not modified with lipids)

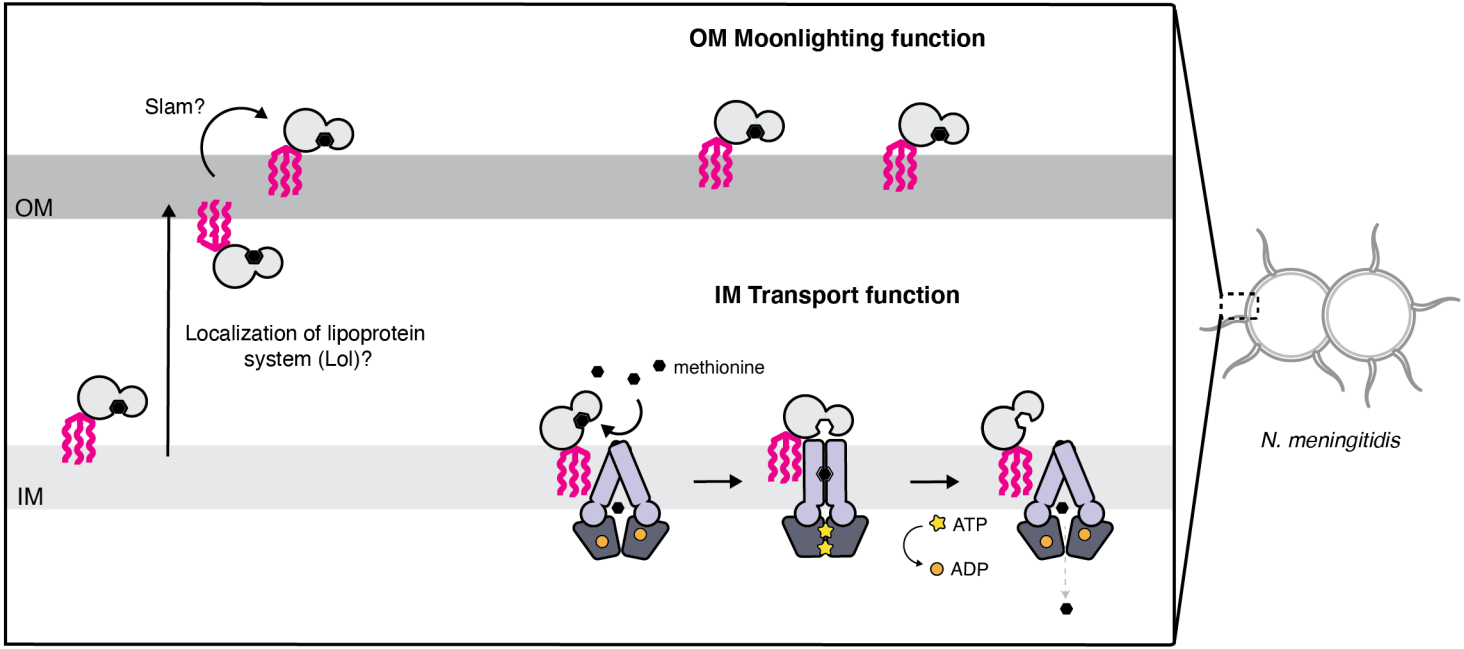
OM Moonlighting function
Slam?
OM
Localization of lipoprotein system (Lol)?
IM Transport function
methionine
IM
ATP
ADP
N. meningitidis